Plant factories

Reducing energy demand at high internal heat loads through façade design

Graamans, Luuk; Tenpierik, Martin; van den Dobbelsteen, Andy; Stanghellini, Cecilia

DOI
10.1016/j.apenergy.2020.114544

Publication date
2020

Document Version
Final published version

Published in
Applied Energy

Applied Energy 262 (2020) 114544

Contents lists available at ScienceDirect

Applied Energy

journal homepage: www.elsevier.com/locate/apenergy

Plant factories: Reducing energy demand at high internal heat loads through façade design

Luuk Graamans[a,b,*], Martin Tenpierik[a], Andy van den Dobbelsteen[a], Cecilia Stanghellini[b]

[a] Faculty of Architecture and the Built Environment, Delft University of Technology, P.O. Box 5043, 2600 GA Delft, the Netherlands
[b] Wageningen UR Greenhouse Horticulture, P.O. Box 644, 6700 AP Wageningen, the Netherlands

HIGHLIGHTS

- We investigate the façade's impact on energy and electricity use in plant factories.
- Lower insulation can reduce cooling demand by 18.8–30.4% through heat dissipation.
- Optimised opaque façades can reduce electricity use for plant factories by 0.3–2.3%
- Transparent façades can reduce electricity use for plant factories by 7.4–9.4%
- We index fundamental strategies for façade construction at high internal heat loads.

ARTICLE INFO

Keywords:
Cooling demand
Data centre
Energy efficiency
Façade design
Urban agriculture
Vertical farm

ABSTRACT

The increase in global food demand has led to the introduction of new food production systems. One key example is the plant factory. Plant factories face the same challenge as many high-tech building functions: high energy demands resulting from high internal heat loads. In this study we investigate how this energy demand can be reduced through façade design. Energy efficient design closely follows function, façade construction and local climate. Therefore, we analysed the effects of façade properties on the energy use in plant factories for three disparate climate zones: Sweden (Dfc), the Netherlands (Cfb) and the United Arab Emirates (BWh). We coupled the building energy simulation program EnergyPlus with a crop transpiration model to calculate the lighting, sensible cooling, latent cooling, and heating demand from the energy balance. In terms of energy demand (kWh m^{-2}), opaque façades with high U-values and optimised albedo can reduce the facilities' cooling demand by 18.8%, 30.0% and 30.4%, and their energy demand by 6.1%, 12.5% and 9.5%, for the United Arab Emirates, the Netherlands and Sweden, respectively. In terms of electricity use (kWhe m^{-2}), transparent façades are more efficient, as they allow the use of freely available solar energy instead of artificial light. These façades can reduce electricity use by 9.4%, 7.6% and 7.4%, for the United Arab Emirates, the Netherlands and Sweden, respectively. The presented façade design strategies can significantly reduce energy demand in plant factories. The investigation provides a foundation for the energy efficient design of high-tech buildings, tailored to local climate.

1. Introduction

1.1. Background

Studies on urban climate resilience have resulted in the development of building typologies with new functions and improved performances. There is a growing interest in technologically advanced facilities for urban agriculture, such as plant factories and vertical farms[1] [1]. These facilities are suggested to increase urban resiliency by ensuring the local supply of fresh food in the face of expanding urban populations. Food is generally supplied to large cities via the global food supply network, but the sustainability and resiliency of this network is questionable [2]. The predominance and complexity of the network will increase further as a result of the projected increase in the global urban population [3] to 6.3 billion by 2050 [4].

An exceptionally high productivity is a prerequisite for the (economic) viability of urban agriculture in view of local food demand and the financial value of urban space. Plant factories are closed production

* Corresponding author at: Architecture and the Built Environment, Delft University of Technology, P.O. Box 5043, 2600 GA Delft, the Netherlands.
E-mail address: L.J.A.Graamans@tudelft.nl (L. Graamans).

[1] As a working definition, a vertical farm can be regarded as a plant factory with multiple building storeys.

https://doi.org/10.1016/j.apenergy.2020.114544
Received 5 September 2019; Received in revised form 4 January 2020; Accepted 19 January 2020

systems which are designed to maximise production density [5], crop productivity [6] and resource use efficiency [7]. Their aim is to increase productivity by stacking production layers and by optimising the interior climate with uniform lighting, temperature, CO_2 concentration and relative humidity. Uniformity is achieved by minimising the interaction with the exterior climate. This limited interaction could also contribute to the efficient (re-)use of energy [8], water [6] and CO_2 [9] in the plant factory, particularly in comparison with standard greenhouses [8].

The evident shortcoming of this typology is the high electricity requirement for artificial illumination to drive photosynthesis. Furthermore, the combination of high-density crop production, limited volume and lack of natural ventilation is likely to result in a high demand for cooling and vapour removal [10]. Sensible cooling, dehumidification and illumination account for approximately 32%, 11% and 57% of the total energy demand, respectively [8]. The high internal heat load and the demand for cooling in plant factories resemble the energy profile of modern data centres [11]. Improving the façade design can reduce the energy demand of plant factories and of other facilities with high internal heat loads. It has already been demonstrated that optimising insulation factors can limit HVAC system energy use [12] and that optimising window properties in conjunction with building form can increase the total energy efficiency of office buildings [13].

Façade design is directly related to context as well as to building design. Contextual factors include location, exterior climate and user behaviour; design factors include the building's shape, orientation, volume, zoning, compartmentalisation and envelope. Energy performance is predominated by the transfer of heat (e.g. insulation: U-value), and solar energy (e.g. solar heat gain coefficient: SHGC).

1.2. Problem statement

The façade design in plant factories differs from that for office buildings and housing, due to the high internal heat load and vapour production associated with plant production. Until now façade research typically has been concerned with the reduction of energy transfer across the façade, in order to limit cooling demands in warm climates [14] or heating demands in cold climates [15], whilst maintaining a certain level of transparency. On the other hand, research in the field of plant factories has been largely concerned with fully opaque, highly insulated and airtight structures [7]. Finally, research on building functions with comparatively high internal heat loads has predominantly focussed on the cooling systems in data centres. Examples range from reviewing the various thermal management techniques [16], to the impact of local climate on cooling system efficiency [17], and the integration of renewable energy [18] in data centres.

Little research has been done on the façade design of buildings with high internal heat loads, such as plant factories or data centres. To bridge that gap, this study addresses the interrelationship between façade properties and total energy demand in plant factories. Moreover, it formulates a rule-of-thumb for façade engineering at high internal heat loads, taking latitude and external conditions into account.

1.3. Objective

The main objective of this study is to quantify the effect of façade construction on the cooling, dehumidification, heating and lighting demand for lettuce production in plant factories, and to analyse how this demand is affected by the external climate.

1.4. Outline and framing

In this study, we have coupled established models for crop transpiration and energy balance to calculate and analyse the energy requirement for lettuce production in closed systems. A total of 54 variations (18 different façade constructions for three different building form factors) have been calculated for three disparate climate zones.

This study seeks to contribute to the energy efficiency of modern buildings. The analyses provide a foundation for the energy efficient design of plant factories and other building functions with high internal heat loads, such as data centres or other industrial functions. To the authors' knowledge, there are numerous studies on active measures to regulate these internal loads, but little is known about passive methods. Additionally, this study seeks to contribute to the field of sustainable food and energy supply. The energetic performance and optimisation of food production in plant factories and their potential integration into metropolitan areas have not yet been investigated in a quantitative manner. In short, this study seeks not only to contribute to the field of building energy efficiency but also to provide perspective on sustainable energy systems, the environmental footprint of cities and potentially climate change mitigation.

2. Materials and methods

The energy use of plant factories in three different locations was analysed. The energy demand of each facility consists of the system demands for dehumidification, sensible cooling, heating and artificial illumination, all of which are influenced by internal and external gains. These demands are calculated and compared using building simulation software.

2.1. Model selection

2.1.1. Building energy simulation

The energy loads and demands were calculated by means of EnergyPlus, using DesignBuilder v5.3. EnergyPlus is a dynamic building energy simulation program that consists of three basic components – a simulation manager, a heat and mass balance simulation module and a building systems simulation module [19]. Formal independent testing has been integral to the development of the model [20]. Afterwards, the model has been used in numerous studies to calculate building energy performance and has been extensively validated, i.e. for the calculation of energy use in large buildings [12], the effect of façade design on the energy use in high-rise buildings [21], the calculation of zone climate loads [22], the simulation of energy flows through windows [23], the use of standard window performance indices to model window energy impacts [24], the impact of normalized energy profiles on hourly building energy consumption [25], as well as the temperature and velocity of air in a double-skin ventilated façade [26]. Furthermore, the climate in EnergyPlus for the selected locations is based on typical meteorological years, in order to guarantee a close representation of typical weather patterns [27]. It should still be realised, however, that "there is no such thing as a completely validated building energy simulation computer program. All building models are simplifications of reality" [28].

DesignBuilder [29] was used to generate input and visualise output, as it is considered the most complete graphic user interface for EnergyPlus. DesignBuilder does not allow for the integration of dynamic processes in order to calculate the effects of plants on the interior climate in real time, such as advanced greenhouse simulation models e.g. KASPRO [30]. This is not a limitation, however, as plant factories have just two states (photoperiod and dark period), each with constant climate setpoints throughout. In order to adequately calculate the interior energetic fluxes, it is essential to calculate the crop energy balance in both states – how it transpires, reflects light and exchanges heat and radiation.

2.1.2. Crop energy balance

The crop energy balance is a key factor in the internal heat load and should therefore be based on an accurate estimate of the crop transpiration coefficient, i.e. the fraction of the radiation flux dissipated by

the crop as latent heat. Cooling and vapour removal are quite different processes and the relation between sensible and latent heat is included in the calculation of energy demand. The energetic behaviour of crops was integrated into the simulations, following the method, model and assumptions described previously [10]. This model was validated for climate setpoints similar to those used in this study (Table 3). An average leaf area index of 2.1 was taken into account for the crop energy balance [31], in order to simulate that all stages of crop development are simultaneously present. The various positive energetic fluxes were set as equipment gains in DesignBuilder; the negative sensible heat fluxes were set as process gains, following the method described in [8].

The inefficiency of the LED-lighting system produces sensible heat, which was also set as an equipment gain. Assuming a system with an efficiency of 2.70 μmol J^{-1} and a red:blue distribution of 80:20, the waste heat is calculated as 48% of the electricity input (in W). The simulated plant factory features a lighting intensity of 250 μmol m^{-2} s^{-1}, which translates to 46.15 W m^{-2} sensible heat per production layer.

2.1.3. Crop production

Minor differences in the interior climate of plant factories can result in differences in plant production and energetic performance. To allow for comparing data across studies, plant production should be calculated. There are several crop models available for the calculation of dry matter production, ranging from extensive and complex (i.e. 3D crop models, incorporating leaf angles and illumination ray tracing [32]), to pure photosynthetic assimilation (i.e. CO_2 assimilation in leaves [33]). To this end, the crop model described by Van Henten [34] was selected and implemented in the computational software MATLAB [35] to calculate plant production, as described earlier [8] and presented in Appendix B. This model reduces the three-dimensional crop canopy to a single plane (cultivation area) and incorporates the fundamental photosynthesis processes as described by the Farquhar model [33]. This reduction increases workability and computational efficiency and is also considered sufficient for the required level of detail for this study.

The crop model was intensively investigated for its key parameters [36] that have been validated using experiments in Dutch greenhouses [34], which feature lower temperatures than are common in plant factories. The potential underestimation of dry matter production at higher temperatures has been investigated and quantified [8]. Therefore, energy demand is normalised for area (m^2) and not for plant production (kg dry matter) throughout most of this study, in order to minimise the effect of this underestimation and to enhance the applicability of the presented findings within the broader field of energy systems engineering.

2.2. Fixed model inputs

2.2.1. Location and typology

Three representative sites of disparate latitudes and climates were selected, namely Kiruna in Sweden (67.8° N, 20.2° E; SWE), Amsterdam in the Netherlands (52.0° N, 5.7° E; NLD) and Abu Dhabi in the United Arab Emirates (24.5° N, 54.7° E; UAE). The hourly weather information for the simulations was retrieved from the EnergyPlus database [37–39], which was selected for its extensiveness and precision. Fig. 1 shows a monthly summary for solar radiation and temperature.

Table 1
Geometry of simulation models.

W/F ratio	–	0.39	0.49	0.65
Length	m	36.00	72.00	108.00
Width	m	36.00	18.00	12.00
Height	m	3.50	3.50	3.50
Floor area	m^2	1296.00	1296.00	1296.00
Wall area	m^2	504.00	630.00	840.00

2.2.2. Interior climate setpoints

This study addresses the climate setpoints that directly influence dry matter production and it does not take the cultivars or other physiological factors into account. The climate setpoints for plant factories had to be carefully selected, as the productivity of lettuce is mainly determined by the relationship between canopy temperature, root zone temperature, photosynthetic photon flux density, photoperiod and CO_2 concentration. The photosynthetic photon flux density (PPFD) describes the number of photons in the photosynthetically active spectrum per square metre per second (μmol m^{-2} s^{-1}), whereas the photoperiod (h d^{-1}) describes its diurnal duration.

This study uses PPFD of 250 μmol m^{-2} s^{-1} as this should result in a high net photosynthetic rate of lettuce leaves [40] and a high light use efficiency [41]. The PPFD is combined with a photoperiod of 16 h d^{-1} to ensure adequate crop production, which is optimised for net photosynthetic rate [40], plant growth [42], light use efficiency [43] and thus for energy consumption. Furthermore, restricting the photoperiod to 16 h d^{-1} should prevent premature bolting [44], which would render the crop unmarketable.

In greenhouses lettuce is usually grown at low temperatures, e.g. 12/9°C for day-/night-time in the Netherlands. In plant factories a low setpoint for air temperature would lead to an unrealistically high cooling demand, due to their high internal heat loads. Therefore, air temperature was maintained between 24 °C and 30 °C as this allows for the highest CO_2 assimilation at the selected PPFD and CO_2 concentration [45]. The relative humidity was maintained at between 75 and 85%. The root zone temperature was set to 24 °C to ensure adequate plant production under elevated air temperatures, i.e. fresh weight production and the formation of compact heads [46]. Total production, colour, thickness and root structure were superior at this root zone temperature, at each air temperature [47].

The typical elevated CO_2 concentration setpoint in plant factories of 1200 ppm was used, in line with [48]. A small supply of CO_2 is considered sufficient to maintain this concentration, as the loss of CO_2 to the exterior climate is minimised in an airtight plant factory.

2.2.3. Geometry

In this study we consider one building type with wall-to-floor ratios (W/F ratios) of 0.39, 0.49 and 0.65 (Table 1). The building height was kept constant at 3.5 m and contains five layers of crop production. This represents a common set-up for contemporary plant factories [7]. The properties of the various building components are listed in Table 2 and 3.

2.3. Variable model inputs

This study focuses on the static façade components and the ratio of wall-to-floor area; we consider 18 façade constructions (opaque and transparent) and three W/F ratios (Tables 1 and 2). The analysis uses single factor variation to illustrate the impact of each factor and to prevent the exclusion of design combinations. This approach allows for an investigation of fundamental aspects that relate to the energy requirements of this novel building typology.

2.3.1. Opaque façade constructions: Insulation and albedo

Two parameters of the opaque façade elements were considered: U-value and surface albedo. The opaque façade was modelled as aluminium panels encapsulating polyurethane foam, as in the construction of cold stores. This is standard practice in plant factories [6].

Insulation: The U-values were set at 0.05, 0.20 and 5.75 W m^{-2} K^{-1}. These values were selected to represent a vacuum insulation panel [49], a standard insulated masonry façade [50] and a thermally conductive metal sheet [51], respectively. A single metal sheet is not considered feasible as a façade construction. However, this construction was

Table 2
Parameters for annual energy demand simulations. Middle values are typically aligned with the current accepted building practice. Variables not considered in a specific simulation set (#) are marked by X. The variables are expanded upon in Section 2.3.

		Form factor	Façade properties				Roof properties	
#	Type	W/F ratio (–)	U-value (opaque)(W m^{-2} K^{-1})	Albedo (–)	U-value (transparent)(W m^{-2} K^{-1})	Solar heat gain coefficient(-)	U-value roof (opaque) (W m^{-2} K^{-1})	Albedo (–)
O1	Opaque – insulation	0.39	0.05 / 0.20 / 5.75	0.50	X	X	0.05 / 0.20 / 5.75	0.50
O2	Opaque – albedo	0.39	5.75	0.10 / 0.50 / 0.90	X	X	5.75	0.10 / 0.50 / 0.90
O3	Opaque – W/F – insulation	0.39 / 0.49 / 0.65	0.05 / 0.20 / 5.75	0.50	X	X	0.05 / 0.20 / 5.75	0.50
O4	Opaque – W/F – albedo	0.39 / 0.49 / 0.65	5.75	0.10 / 0.50 / 0.90	X	X	5.75	0.10 / 0.50 / 0.90
T1	Transparent – insulation	0.39	X	X	0.50 / 0.20 / 5.75	0.55	0.20	0.50
T2	Transparent – SHGC	0.39	X	X	5.75	0.30 / 0.50 / 0.80	0.20	0.50
T3	Transparent – W/F – insulation	0.39 / 0.49 / 0.65	X	X	0.50 / 0.20 / 5.75	0.55	0.20	0.50
T4	Transparent – W/F – SHGC	0.39 / 0.49 / 0.65	X	X	5.75	0.30 / 0.50 / 0.80	0.20	0.50

Table 3
Constant model input for annual energy demand simulations.

Climate setpoints		Climate systems		Building components	
Parameter	Input	Parameter	Input	Parameter	Input
Location	SWE: 67.83° N, 20.34° E NLD: 51.99° N, 5.66° E UAE: 24.45° N, 54.65° E	HVAC system (template)	Fancoil unit Air cooled chiller	Façade construction (opaque)	1-Layers Aluminium[c] – PUR[d] – Aluminium
ASHRAE/Köppen-Geiger climate classification	SWE: 7/Dfc NLD: 4A/Cfb UAE: 1B/BWh	Lighting system	LED	Façade lay-out (opaque)	No glazing
Heating setpoints photo-/dark period (°C)	24/24[a]	HVAC – Fuel heating	1-Electricity from grid	Façade construction (transparent)	2-Simple glazing[e]
Cooling/ventilation setpoints photo-/dark period (°C)	30/30[a]	HVAC – Fuel cooling	1-Electricity from grid	Façade lay-out (transparent)	100% fitted glazing
Relative humidity setpoints photo-/dark period (%)	RH_{min} = 75/75[a] RH_{max} = 85/85[a]	HVAC – COP heating	1.00[b]	Ground floor	150 mm concrete slab 30 mm XPS
CO_2 levels (µmol mol^{-1})	1200[a]	HVAC – COP cooling	1.00[b]	Internal floor	300 mm concrete slab
Radiation (µmol m^{-2} s^{-1})	250[a]	HVAC – Humidification	2-Humidistat	Internal thermal mass	300 mm concrete slab
Duration photo-/dark period	16 h/8h[a]	HVAC – Dehumidification	2-Humidistat	Air tightness	Model infiltration off[f]

[a] The interior climate setpoints are expanded upon in Section 2.2.2.
[b] COPs were calculated separately (see Section 2.4).
[c] Exterior surface properties were varied to achieve desired albedo (see Section 2.3.1).
[d] PUR Polyurethane board (diffusion tight). Thickness was varied to achieve desired U-value.
[e] Glazing properties were varied to achieve desired solar heat gain coefficient and U-value. Light transmission was fixed at 0.70.
[f] Standards for airtightness were exceeded to simulate a fully closed system [7].

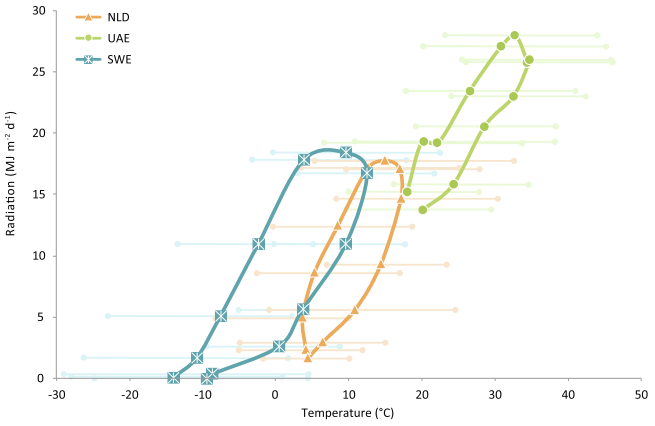

Fig. 1. Average daily radiation per month (MJ m^{-2} d^{-1}) and monthly average, minimum and maximum temperatures (°C) for Kiruna (SWE, stars), Amsterdam (NLD, triangles) and Abu Dhabi (UAE, circles). January is the lower left data point in each cycle.
Adapted from [8]

selected in order to achieve the same U-values as single layer clear glazing (see Section 2.3.2). Heat transmission is limited by increasing the insulator thickness, as is common practice with conventional insulation materials. A more space-efficient, innovative method to increase the performance of the building skin would consist of more efficient insulation materials, such as vacuum insulation panels [52], aerogels [53] or nanomaterials [54].

Surface albedo: The albedo values were set at 0.10, 0.50 and 0.90. Surface albedo is defined as the ratio of the irradiance reflected from a surface to the irradiance received by that surface. In warm areas, low albedo values can result in high surface temperatures. The selected values represent the available range for building materials [55]. To be able to distinguish between results, the impact of albedo was calculated for a U-value of 5.75 W m^{-2} K^{-1}.

Roof: The albedo and U-value of the roof are in accordance with the façade for each simulation. The effect of this approach is discussed in Section 4.5.

Operation: The daily photoperiod inside was in counter phase with the natural photoperiod (photoperiods last from 18:00–10:00^{+1}) in order to maximise heat transmission across the façade. This schedule maximises the temperature difference between the interior and exterior during both photoperiods and dark periods. During photoperiods, the high internal heat load corresponds with exterior night-time temperatures to maximise heat loss. During dark periods, the elevated exterior daytime temperatures can reduce heating demands.

2.3.2. Transparent façade constructions: Insulation and solar heat gain coefficient

Two parameters of the transparent façade elements were considered: U-value and solar heat gain coefficient (SGHC). The U-value and SGHC of the façade constructions have a double influence on the interior climate. Fully transparent façades increase the penetration of solar radiation, which can contribute to crop production. Conversely, they increase solar heat gains and thermal emission, thereby increasing the cooling and heating requirements, respectively. The transparent façade was modelled as a curtain wall system with glass panels consisting of single or multiple layers, using the simple glazing method of DesignBuilder [24].

Insulation: The U-values were set at 0.50, 1.25 and 5.75 W m^{-2} K^{-1}, representing triple, double and single glazing, respectively [50]. They take the frame and connection between glazing and frame into account.

SHGC: The SHGC of the transparent façade was set at 0.30, 0.55 and 0.80. The SHGC is the ratio of the transmitted solar radiation to the incident solar radiation on the entire glass façade, including the window frames. Emissivity and transmissivity of the façade are included in SHGC (total transmission) when using the simple glazing method and are not independently defined [56,57].

Roof: The roof was modelled as an opaque element, featuring the medium albedo and U-values of 0.5 and 0.20 W m^{-2} K^{-1}, respectively. This was done to prevent modelling a structure akin to a greenhouse.

Operation: Contrary to the opaque façade, the daily photoperiod follows the natural exterior photoperiod to maximise the use of photosynthetically active solar radiation; photoperiods last from 04:00–20:00.

Integrating natural and artificial illumination: The daily photoperiod inside follows the natural photoperiod (photoperiods last from 05:00–21:00). A combination of artificial illumination and solar radiation must be taken into account, as solar radiation is neither continuous nor capable of fully penetrating the building structures. In this study it was assumed that solar illumination levels were continuously supplemented to 250 µmol m^{-2} s^{-1}. The calculated solar gains were subtracted from the lighting requirement and the consequent sensible cooling requirement when processing the hourly simulation data.

2.3.3. Form factor: wall-to-floor area ratio

The geometrical form affects the relative surface area and consequently the influence of the façade on the building energy balance. Therefore, this study took three rectangular W/F ratios (Table 1) into account to obtain a fundamental understanding of this influence. The floor and roof surface area remained constant. The production and logistic aspects of the facility layouts were not taken into consideration.

2.4. Climate systems – Energy demand and electricity use

The individual energy demands for the climate systems are a direct output from DesignBuilder. The system demands are converted to electricity use by using their respective coefficients of performance (COP). The COP of a climate system is the ratio of the generated flux (i.e. sensible heat or refrigeration) to the net input of work (electricity) required to achieve that effect.

The COP for heating (COP_{heat}) was determined using the Carnot efficiency of a heat pump. This theoretical optimum efficiency was multiplied by 0.4 to achieve realistic efficiencies, following [58].

In addition, the COP was determined for sensible and latent cooling, as these play a central role in the total energy balance of plant factories. To reduce electricity use, cooling is achieved through a combination of active and 'free' cooling. 'Free' cooling uses the temperature difference between the interior and the exterior climate and bypasses the need for compressors [59]. The exterior climate naturally determines the number of hours that free cooling can be used [11].

In this study, active cooling was realised by a vapour compression refrigeration cycle. Air-to-air heat exchangers were used to minimise the use of vapour compression cooling and consequently the electricity

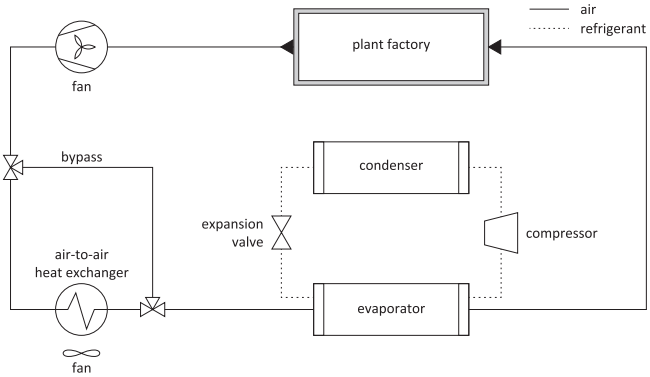

Fig. 2. Schematic representation of the cooling system design. A continuous line represents the flow of air and a dashed line the flow of the refrigerant.

demand for cooling and dehumidification (Fig. 2). The methods for calculating the air extraction, heat exchanger and vapour compression cooling systems are detailed in Appendix C. An indirect system is used as this causes no direct disturbance to the indoor air quality and does not introduce vapour or other volatiles into the production climate.

The potential of natural circulation using a thermosyphon was investigated, as it has the capability to transport heat at high rates without needing pumping devices [60]. The system, however, was not considered suitable for this study due to numerous uncertainties: the dimensioning of components [61], the heat transfer limit due to pressure drops [62], the impact of pipe dimensions [63], the limited experimentally validated cooling capacities [64], and the overall refrigerant flow stability [65].

Electricity demand

The total electricity demand for plant factories (E_{PF}) is comprised of the electricity demand for heating (E_H), dehumidification or latent cooling (E_{lat}) and sensible cooling (E_{sen}). Additionally, the energy required for cooling the nutrient solution (E_{NS}) and for powering the LED fixtures (E_{LED}) were included.

$$E_{PF} = E_{heat} + E_{lat} + E_{sen} + E_{NS} + E_{LED} \quad (1)$$

The system demands (Q_a) for plant factories are converted to electricity use (E_a) following their respective COP (COP_a) according to the formula:

$$E_a = \frac{Q_a}{COP_a} \quad (2)$$

The electricity demand E_{heat}, E_{lat} and E_{sens} are calculated using the COP for heating (COP_{heat}) and cooling (COP_{cool}), respectively. Additionally, the required electrical fan power (E_{fans}) is included, weighted for the relative share of the heating flux (Q_H), latent cooling flux (Q_{lat}) or sensible cooling flux (Q_{sens}) in the combined energy demand ($Q_{heat} + Q_{lat} + Q_{sens}$).

$$E_{heat} = \frac{Q_{heat}}{COP_{heat}} + \frac{Q_{heat}}{Q_{heat} + Q_{lat} + Q_{sens}} \cdot E_{fans} \quad (3)$$

Additionally, the required electrical fan power from the heat exchanger ($E_{fans,hex}$) is included and weighted for the latent and sensible flux in the heat exchanger ($Q_{hex,lat}$ and $Q_{hex,sens}$, respectively).

$$E_{lat} = \frac{Q_{lat}}{COP_{cool}} + \frac{Q_{lat}}{Q_{heat} + Q_{lat} + Q_{sens}} \cdot E_{fans} + \frac{Q_{hex,lat}}{Q_{hex,lat} + Q_{hex,sens}} \cdot E_{fans,hex} \quad (4)$$

$$E_{sens} = \frac{Q_{sens}}{COP_{cool}} + \frac{Q_{sens}}{Q_{heat} + Q_{lat} + Q_{sens}} \cdot E_{fans} + \frac{Q_{hex,lat}}{Q_{hex,lat} + Q_{hex,sens}} \cdot E_{fans,hex} \quad (5)$$

2.5. Presentation of the results

The analysis of energy-saving potential was carried out by comparing several scenarios. As a starting point, simulations were carried out considering the industry standard: an opaque, highly insulated (U = 0.05 W m^{-2} K^{-1}), moderately reflective (A = 0.50), square (W/F = 0.39) plant factory. Results are reported in absolute and relative values on an annual basis (kWh m^{-2} y^{-1}).

3. Results

The results have been normalised for cultivation area (Section 4) and for dry matter production (Appendix B). The total annual energetic demands for opaque and transparent façades are specified in Figs. 3 and 4, respectively. The energy requirements were calculated for each plant factory and specify the energy use for LED lighting, sensible cooling, dehumidification and heating. The total energy use is reduced in opaque and transparent façades by increasing U-values. SHGC reduces the total energy use at varying intensities in different locations, whereas the effect of albedo is more closely related to location. Figs. 5 and 6 illustrate the impact of form factor (W/F ratio) on the total annual energetic demands for opaque and transparent façades, respectively. Increasing the W/F ratio consequently increases the impact of the façade components on the total energy use. This impact can result in additional energy savings. Total energy use is closely related to the differences between the interior and the exterior climate. Finally, Fig. 7 gives an overview of the energy and electricity use of the most efficient analysed systems. The COP of the different systems is used to convert energy demand to electricity use. The predominance of electricity required for artificial illumination is illustrated.

4. Discussion

The following section discusses the calculated energy demands per cultivation area (kWh m^{-2}). The figures illustrate the impact of each single variable for each location.

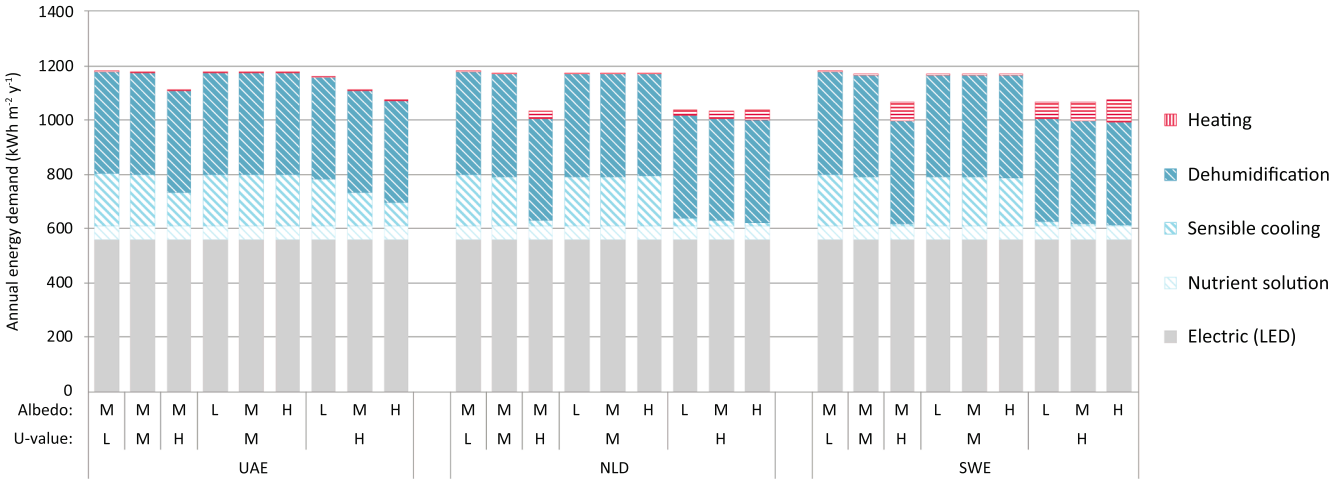

Fig. 3. Annual energy demand (kWh m^{-2} y^{-1}) of plant factories featuring opaque façades in UAE, SWE and NLD, as a result of variation in insulation (U-value in W m^{-2} K^{-1}) and reflection of solar radiation (albedo). Values are indicated by L (low: A = 0.10, U = 0.05), M (medium: A = 0.50, U = 0.20) and H (high: A = 0.90, U = 5.75) and refer to values listed in Table 2. Presented simulations feature a W/F ratio of 0.39 and face north.

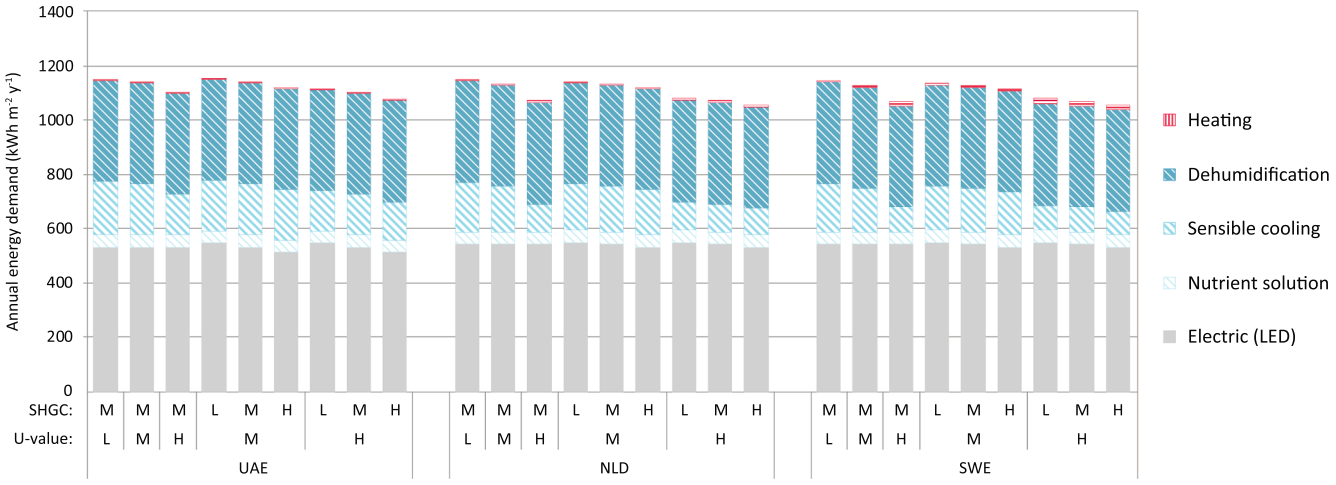

Fig. 4. Annual energy demand (kWh m^{-2} y^{-1}) of plant factories featuring transparent façades in UAE, SWE and NLD, as a result of variation in insulation (U-value in W m^{-2} K^{-1}) and solar heat gain coefficient (SHGC). Values are indicated by L (low: SHGC = 0.30, U = 0.50), M (medium: SHGC = 0.55, U = 1.25) and H (high: SHGC = 0.80, U = 5.75) and refer to the values listed in Table 2. Presented simulations feature a W/F ratio of 0.39 and face north.

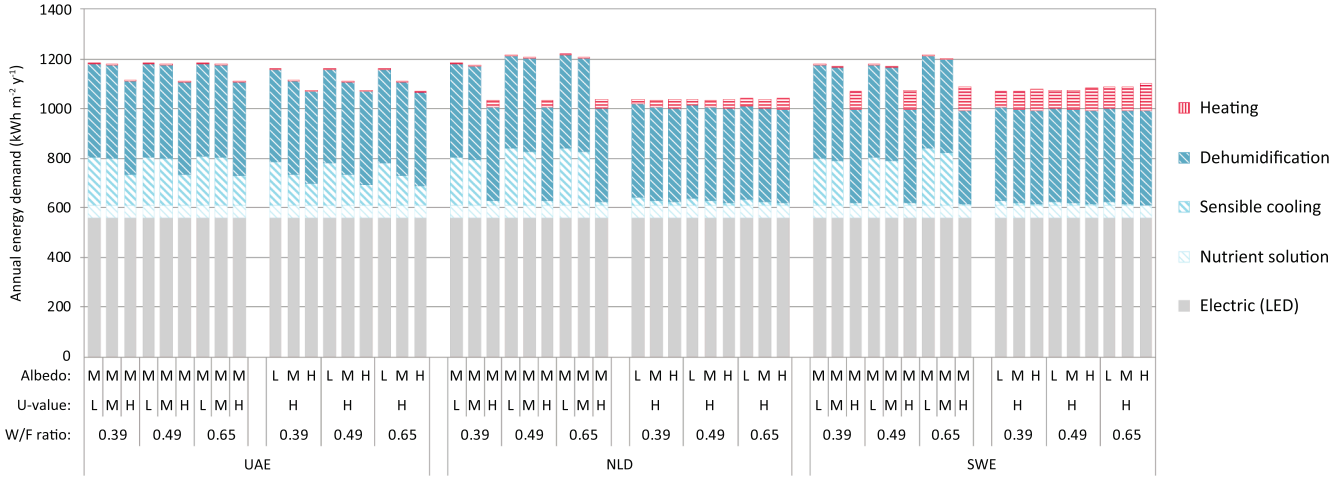

Fig. 5. Annual energy demand (kWh m^{-2} y^{-1}) of plant factories in UAE, NLD and SWE featuring opaque façades, as a result of variation in insulation (U-value in W m^{-2} K^{-1}) and reflection of solar radiation (albedo) in combination with W/F ratio. Values are indicated by L (low: A = 0.10, U = 0.05), M (medium: A = 0.50, U = 0.20) and H (high: A = 0.90, U = 5.75) and refer to values listed in Table 2. The long façade faces north in presented simulations.

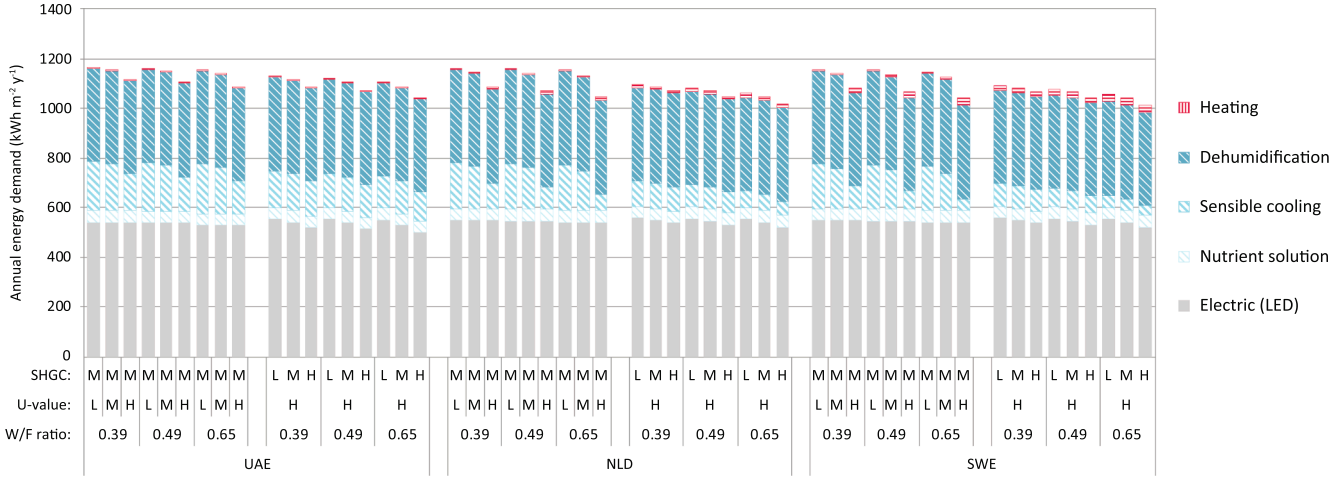

Fig. 6. Annual energy demand (kWh m^{-2} y^{-1}) of plant factories in UAE, NLD and SWE featuring transparent façades, as a result of variation in insulation (U-value in W m^{-2} K^{-1}) and solar heat gain coefficient (SHGC) in combination with W/F ratio. Values are indicated by L (low: SHGC = 0.30, U = 0.50), M (medium: SHGC = 0.55, U = 1.25) and H (high: SHGC = 0.80, U = 5.75) and refer to the values listed in Table 2. The long façade faces north in presented simulations.

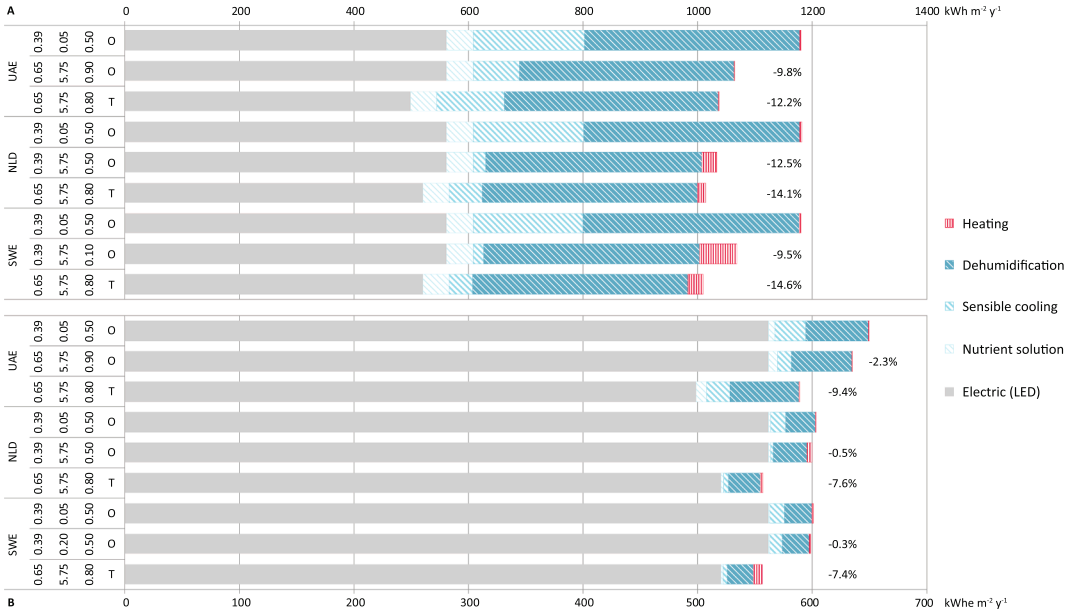

Fig. 7. Energy demand (A) in kWh m^{-2} y^{-1} and final electricity use (B) in kWhe m^{-2} y^{-1} for the most efficient opaque and transparent constructions in each location. The relative delta (%) illustrates the difference with the industry-standard plant factory in the specific location (opaque, U = 0.05 W m^{-2} K^{-1}, A = 0.55, W/F = 0.39). The y-axis lists location, W/F ratio (-), U-value (W m^{-2} K^{-1}), SGHC (–) or albedo (–) (dependent on transparency), and transparency (O for opaque and T for transparent) from left to right. The long façade faces north in presented simulations.

4.1. Opaque façade constructions

4.1.1. Opaque façade constructions – Insulation values

The effects of the opaque façades' insulation and albedo on the total energy demand are illustrated in Fig. 3. The plant factories show a decrease in energy demand resulting from higher U-values. Increasing the façades' U-value from 0.05 to 5.75 W m^{-2} K^{-1} changes the facility's total cooling demand by –12.1% (UAE), –30.0% (NLD) and –31.6% (SWE) and its total energy demand by –6.1% (UAE), –9.5% (SWE) and –12.5% (NLD).

The decrease in sensible cooling demands indicates an increased heat transmittance from the interior to the exterior climate. These effects are most pronounced in the decrease of total energy demand in cooler climates, such as NLD and SWE, but are also seen in UAE. In all locations the savings related to the sensible cooling demand were notably higher than the increase in heating demand.

4.1.2. Opaque façade constructions – Albedo values

The effect of the albedo of total energy demand is closely related to the facility's location and the façade's U-value (Fig. 3). The albedo value had hardly any effect at the medium U-value, as the thermal insulation limits most heat transmittance across the façade. However, increasing the albedo value from 0.1 to 0.9 at the highest U-value resulted in maximum changes in total energy demand of +0.8% (SWE), –0.5% (NLD) and –7.5% (UAE).

The effect of the albedo value is visible in the heating and sensible cooling demands and is notably dependent on location. In general, lower albedo values will increase the exterior surface temperature, which results in a decreased heat transmittance to the exterior and a higher sensible cooling demand. Concomitantly, at lower albedo values the heating demand is reduced due to the increased heat gain from the exterior walls. The most notable decrease in total energy demand is achieved at the maximum albedo value in UAE, as the high exterior temperatures in UAE reduce the need for heating. The high internal heat load and temperature setpoints still allow for the dissipation of energy. In contrast, albedo has a clearer effect on the heating demand than on the sensible cooling demand in SWE.

The façade albedo values have a smaller impact on the total energy demand than the insulation values, but they show distinct trends related to the exterior climate. This observation allows for additional fine-tuning of the façade construction to the local climate, aiming at a further reduction of the total energy demand.

4.2. Transparent façade constructions

In all locations the energy demands calculated for artificial illumination exceed all other demands (Fig. 3). This predominance of artificial illumination in the total energy balance is consistent with data from a wide range of production climates (i.e. 50.1% [66], 72.0–86.0% [67], 75.0–80.0% [68], 42.8–52.6% [69], and 57.0–57.4% [8]). Transparent façades may serve to reduce electricity costs by directly using solar energy and limiting artificial illumination. In reality, the values for insulation and SHGC are largely linked. However, greater insight into the energetic behaviour can be achieved by independently assessing both factors.

4.2.1. Transparent façade constructions – Insulation values

The effects of the transparent façades' insulation and SHGC on the total energy demand are illustrated in Fig. 4. Plant factories show a decrease in total energy demand following higher U-values for transparent façades; increasing the U-value from 0.50 to 5.75 W m^{-2} K^{-1} results in a change in energy demand of –4.2% (UAE), –6.3% (NLD) and –6.4% (SWE).

The lower energy demand at higher U-values is caused by decreased sensible cooling demands, comparable with the situation in the opaque façade structures. The internal heat is partially dissipated across the façade to the exterior climate. In comparison with the opaque structures, the sensible cooling demand changes slightly in UAE (+43%) but notably in NLD (+512%) and in SWE (+1025%) at a U-value of 5.75 W m^{-2} K^{-1}. The combination of the additional solar heat gains and the regular production schedule resulted in an increased transmission of heat across the façade to the interior.

4.2.2. Transparent façade constructions – Solar heat gain coefficient

The impact of SHGC on the total energy demand is related to location and follows the same trend, regardless of the insulation value

(Fig. 4). Increasing the SHGC from 0.3 to 0.8 at a high U-value changes the total energy demand by −2.3% (SWE), −2.4% (NLD) and −3.6% (UAE).

The higher SHGC allows for an increased transmittance of solar radiation, which most notably reduces the need for LED illumination. The savings in total energy demand directly follow the savings in LED energy demand, as the influence on LED was notably higher than the influence on sensible cooling, dehumidification and heating in all locations.

4.3. Geometry – wall-to-floor ratio

In the previous calculations the opaque façade exceeded the transparent façades in energetic performance for SWE and NLD, despite the free availability of solar radiation for photosynthesis. These calculations used a model with a square footprint and minimal relative façade area, which consequently minimised the effect of design variations. The effect of different W/F ratios on the total energy demand in opaque and transparent constructions was addressed. Firstly, the effect of different U-values was analysed; secondly, the impact of albedo value or SHGC was analysed. The W/F ratio of 0.39 (square footprint) was taken as the baseline for comparison.

4.3.1. Geometry – opaque façade constructions

The effect of the W/F ratio on the total energy demand in opaque plant factories depends strongly on the location (Fig. 5). Higher W/F ratios and U-values result in a notably higher total energy demand in NLD and SWE, whereas only minimal differences were seen in UAE. The determining factor for opaque façades is the thermal transmission, which increases at greater temperature differences. These differences are considerably larger in SWE and NLD than in UAE, as is evident in the increased heating demand in NLD and SWE.

In opaque constructions an increase in the W/F ratio generally results in an increase in total energy demand, except in UAE. There, in combination with a high U-value and albedo, the larger façade surface area facilitates additional heat loss during night-time and changes the total energy demand by −0.7%. In UAE the reduction in sensible cooling is greater than the increase in heating, whereas in NLD and SWE the increase in heating remain dominant over the reduction in cooling.

4.3.2. Geometry – transparent façade constructions

A higher W/F ratio results in a decrease in total energy use in the calculated variants, where the longest façade faces north. This effect is more evident in transparent than in opaque constructions, due to the benefits of direct solar radiation. The total energy demand is most notably reduced in the cases focusing on SHGC. Increasing the W/F ratio resulted in a relative change in energy demand of –4.2% for UAE, –5.0% for NLD and –5.2% for SWE with respect to their base value. These energy savings are the result of the lower energy demand for LEDs and lower sensible cooling demands.

The W/F ratio has the highest absolute and relative impact on lighting demand in UAE, followed by SWE and then NLD; the sensible cooling demand was reduced primarily in SWE, followed by NLD and UAE. This decrease in sensible cooling demand at higher SHGCs seems unexpected based on increased solar heat gains. However, the production temperature is higher than the average exterior temperature, which ensures the transfer of heat across the façade. This large decrease in sensible cooling outweighs the absolute increase in heating requirements.

4.4. Comparison of results and sensitivity analysis

The analysed design variables have been applied to minimise the total use of energy and electricity (Table 4 and Fig. 7). These designs might not be economically feasible, but they present the highest potential for energy savings. Additionally, a sensitivity analysis using single variable variation provides insight into the key design factors (Fig. 8).

4.4.1. Comparison of façade properties

The ranges of reduction in annual energy demand are given in Table 4. The table lists the effect of each façade property on the annual energy demand of plant factories at the W/F ratios. The delta is relative to the annual energy demand of the baseline facility, which features the listed properties. Among the analysed variables, the U-value brought about the largest reduction in energy demand, followed by SHGC. The constructions in each location required a high U-value to maximise the dissipation of the internal heat and a high SHGC to minimise LED energy use. However, they notably differ with respect to the W/F ratio and the albedo value. The positive effects of albedo were most evident in UAE and rather minimal in NLD and SWE. The advantage of transparent versus opaque constructions depends on which outcome measure is selected, total energy demand or final electricity use. The latter depends on the COPs of the subsystems.

If energy demand is considered as the outcome measure, the transparent constructions offer the best performance by a narrow margin (Fig. 7A). The opaque constructions already offer a notable reduction in total energy demand. The relatively high external temperature and solar radiation in UAE require a high W/F ratio to allow for (night-time) dissipation of heat and a high albedo to minimise solar heat gains, respectively. In contrast, a small W/F ratio impedes excessive heat losses to the exterior in the colder climates of NLD and SWE. Moreover, medium and lower albedo values allow for increased solar heat gains that minimise heating demands at a U-value of 5.75 W m^{-2} K^{-1} in NLD and SWE, respectively.

If final electricity use is considered as the outcome measure

Table 4
Range of effects of façade properties on the annual energy demand of plant factories. Colour intensity illustrates the relative effect in comparison with the baseline per location. The characteristics of these baselines are given by listing their U-value (U), albedo or solar heat gain coefficient (A or SHGC), and wall-to-floor ratios (W/F). In addition, the transparency (T) is listed and indicated by transparent (T) or opaque (O). The effect of orientation is relative to the north-facing orientation for each W/F ratio (Δ).

Façade construction	Base				UAE			NLD			SWE		
	U	A or SHGC	W/F	T	0.39	0.49	0.65	0.39	0.49	0.65	0.39	0.49	0.65
Opaque: U-value (0.05-5.75)	0.05	0.50	0.39	O	0.0% - 6.1%	+ 0.1% - 6.2%	+ 0.3% - 6.4%	0.0% - 12.5%	+ 2.9% - 12.5%	- 3.0% - 12.3%	0.0% - 9.5%	0.0% - 8.9%	+ 3.0% - 7.8%
Opaque: Albedo (0.10-0.90)	5.75	0.10	0.39	O	0.0% - 7.5%	- 0.1% - 7.7%	+ 0.1% - 8.1%	0.0% - 0.5%	0.0% - 0.5%	+ 0.4% - 0.3%	+ 0.8% 0.0%	+ 1.6% + 0.6%	+ 3.0% + 1.8%
Opaque: Orientation (0°-135°)	5.75	0.50	Δ	O	0.0% 0.0%	+ 0.2% 0.0%	+ 0.3% 0.0%	0.0% 0.0%	+ 0.1% 0.0%	+ 0.1% 0.0%	0.0% 0.0%	+ 0.1% 0.0%	+ 0.1% 0.0%
Transparent: U-value (0.50-5.75)	0.50	0.55	0.39	T	0.0% - 4.2%	- 0.2% - 5.1%	- 0.6% - 6.7%	0.0% - 6.3%	- 0.3% - 7.7%	- 0.8% - 9.8%	0.0% -6.4%	- 0.3% - 7.9%	- 0.8% - 10.1%
Transparent: SHGC (0.30-0.80)	5.75	0.30	0.39	T	0.0% - 3.6%	- 0.8% - 5.0%	- 1.9% - 7.6%	0.0% -2.4%	- 1.3% - 4.3%	- 3.1% - 7.2%	0.0% -2.3%	- 1.4% - 4.4%	- 3.3% - 7.4%
Transparent: Orientation (0°-135°)	5.75	0.80	Δ	T	0.0% 0.0%	0.0% - 0.7%	0.0% - 1.4%	+ 0.1% 0.0%	0.0% 0.0%	+ 0.1% 0.0%	0.0% 0.0%	+ 0.1% 0.0%	+ 0.2% 0.0%

Fig. 8. Sensitivity analysis illustrating the relative change in total energy demand (y-axis) as a result of relative change in LED efficiency, U-value, and albedo or SHGC, respectively (x-axis) in UAE, NLD and SWE. The base values for these parameters are 52% LED efficiency (red:blue = 80:20, 2.70 μmol J^{-1}) for opaque – LED efficiency, 2.90 W m^{-2} K^{-1} for opaque – U–value, 0.50 for opaque – albedo, 3.215 W m^{-2} K^{-1} for transparent – U–value, and 0.55 for transparent – SHGC.

(Fig. 7B), transparent constructions offer the best perspective. The role of illumination becomes more predominant in the final electricity use because of the system COPs. Consequently, this increased predominance increases the relative effects of solar radiation on electricity use. The final electricity use decreases inversely to the W/F ratio and the SHGC as both factors increase the solar gains.

4.4.2. Sensitivity analysis of key variables

The sensitivity analysis provides insight into the variations in total energy demand as a result of the variation in key variables. This sensitivity is closely related to location (Fig. 8). The investigated variables are U-value and SHGC in the case of transparent constructions and LED efficiency, U-value and albedo in the case of opaque constructions. Total energy demand is most sensitive to LED efficiency, followed by U-value.

The impact of LED efficiency was calculated in combination with an opaque façade (U = 5.75 W m^{-2} K^{-1}, A = 0.50). Increasing LED efficiency had a direct effect on the energy demand of illumination and an indirect effect on the sensible cooling and heating demand. Differences in sensitivity across locations illustrate the influence of local climate. The high exterior temperatures in UAE limit the required increase in heating demand, even at reduced internal heat gains. In contrast, the lower exterior temperatures in SWE and NLD result in a decline in sensitivity as LED efficiency increases, because of a larger heating demand.

The impact of U-value was calculated for transparent and opaque constructions. Opaque constructions showed greater variation at U-values varying between 0.05 and 5.75 W m^{-2} K^{-1}. The sensitivity is minimal in UAE due to the relatively limited thermal exchange as a result of high interior temperatures. In contrast, SWE and NLD show greater sensitivity to U-value because of their colder exterior climates. The sensitivity in SWE indicates an optimum U-value (around 4.33 W m^{-2} K^{-1}) due to the shift in predominance of sensible cooling to heating demand. This shift in predominance is responsible for a decline in sensitivity at higher U-values.

The impact of albedo on the total energy demand may be rather small but was clearly influenced by the external climate. Facilities at low latitudes require a high albedo (UAE), moderate latitudes a moderate albedo (NLD) and high latitudes a low albedo (SWE).

In short, the sensitivity analysis illustrates that the general trends are similar for each location. However, the slope and optimum of each variable are closely related to the external climate and warrant future optimisation studies.

4.5. Additional factors affecting energetic performance

Several additional factors that affect the energetic performance of plant factories can be identified. The impact of these factors is described below.

- *The roof as the fifth façade:* In this study, the roof can be regarded as the fifth façade, as it follows the characteristics of the opaque façade. This design approach mirrors the current building practice for plant factories but inhibits the direct extrapolation of the results to a facility with multiple building layers, a vertical farm. To simulate a multi-layered facility, it would be necessary to exclude heat transfer across floors and roofs by modelling them as adiabatic. These additional calculations were beyond the scope of this study.
- *Opaque roof in combination with transparent façades:* In the analysis of transparent façade constructions, the roof was modelled as an opaque element, featuring the medium albedo and U-values of 0.5 and 0.20 W m^{-2} K^{-1}, respectively. However, the analysis of opaque structures indicated the benefits of a roof construction with a U-value of 5.75 W m^{-2} K^{-1}. Additional calculations would be required to assess this combination but were beyond the scope of this study.
- *Orientation of the building:* The beneficial effects or solar radiation can be increased by taking the combination of the W/F ratio and the spatial orientation of the building into account. Changing the orientation from north with 45° increments resulted in maximum changes in total energy demand of –1.4% (UAE) in the case of a transparent plant factory (U = 5.75, SHGC = 0.8, W/F = 0.65). The decrease in LED lighting exceeds the increase in sensible cooling demand in this case. Building orientation has a small influence on total energy use in comparison with façade construction, particularly in NLD and SWE. However, it remains an interesting variable, as it can reduce energy demand but has a negligible effect on the investment costs.
- *Coefficients of performance:* The COPs achieved in practice will strongly influence the final electricity use of the plant factory. The coefficient was calculated for each case (Section 2.4). The COP for cooling in UAE is relatively high due to small differences between the required source temperature and the temperature inside the plant factory. The counter phase production schedule warrants low exterior air temperatures that can be used for passive cooling during night-time. Cooling in SWE might be problematic due to frost on the air chiller during winter time; this would result in a lower COP.
- *LED efficiency:* The sensitivity analysis illustrates the impact of the

efficiency of artificial illumination on the total energy demand and consequently the technoeconomic feasibility of plant factories (Fig. 8). The technological advancement of LED efficiency is of paramount importance, but presumably this is not sufficient to guarantee feasibility. It has to be taken into account that the maximum attainable efficiency ($W_{Output}/W_{Electricity}$) of LEDs is limited [70].

- *Local production of energy:* Photovoltaic cells could be a source of renewable electricity for plant factories. However, the direct use of solar energy is more efficient for crop illumination compared to artificial illumination powered by photovoltaic arrays. This can be illustrated by successively calculating the current efficiencies of photovoltaic arrays at approximately 17% [71] and of LED systems at approximately 52% [72].

4.6. Additional considerations

DesignBuilder exhibited anomalous behaviour in the simulation of simple glazing systems, which resulted in an apparent connection between the U-value of single glass and the transmitted solar gains. This is the result of the glazing 2-Simple method option, where DesignBuilder uses the EnergyPlus object *WindowMaterial:SimpleGlazingSystem*. This object accesses a model that turns simple performance indices into a more extensive model of the glazing system. The overall glazing system is defined using just three parameters: U-value, solar heat gain coefficient, and visible transmittance [56], following the method outlined in [24]. Within the scope of this study, this resulted in a difference of 5.4% between solar gains transmitted through single glazing ($U = 5.75\ W\ m^{-2}\ K^{-1}$) and double/triple glazing ($U = 0.50/1.25\ W\ m^{-2}\ K^{-1}$) at a SHGC of 0.80. The simulation of a broader range of U-values (0.10–7.00 $W\ m^{-2}\ K^{-1}$) demonstrated that this anomaly arose at U-values from 5.75 $W\ m^{-2}\ K^{-1}$ on. It was corrected by substituting the solar gains of insulated glass ($U = 0.50/1.25\ W\ m^{-2}\ K^{-1}$) by those of uninsulated glass ($U = 5.75\ W\ m^{-2}\ K^{-1}$). As a result, the transmission of solar gains exclusively corresponds with SHGC.

5. Conclusions

Research on buildings with a high internal heat load generally concerns the optimisation of equipment efficiency to improve the facility's energy efficiency as a whole. However, the potential of building design and engineering are important as well, as they can contribute to substantial savings with respect to total building energy use. Therefore, this work investigated the total energy demand of plant factories in relation to façade design and exterior climate. Their energy demand was calculated with respect to diverse latitudes and climates: Sweden, the Netherlands and the United Arab Emirates.

On average, the energy demand consists of 50% for lighting, 2% for heating, 34% for dehumidification and 14% for sensible cooling. The insulation (U-value) was found to be the most effective in reducing the total energy demand at every wall-to-floor ratio and in each location (Table 4). In opaque constructions the increase in U-value from 0.05 to 5.75 $W\ m^{-2}\ K^{-1}$ can change the total energy use by –7.1% to –12.5%. Varying the albedo between 0.1 and 0.9 can result in additional change of –0.3% to –8.1%, depending on location. In transparent constructions an increase in U-value from 0.50 to 5.75 $W\ m^{-2}\ K^{-1}$ can contribute –4.2% to –10.1%. Increasing the solar heat gain coefficient from 0.3 to 0.8 was found to change the total energy demand by an additional −2.3% to –7.6%.

The standard practice for plant factories has focused on achieving high insulation values to improve energy use efficiency, regardless of the local climate. Conversely, this study shows that a decentralised dissipation of the internal heat load through the façade can result in a lower total energy demand in each climate that was investigated.

The standard practice for sustainable building focuses on producing compact buildings to minimise both the surface area and the influence of the façade in the total energy balance. Conversely, this study shows that altering the wall-to-floor ratio of the building can amplify the targeted positive effects of the façade construction in certain locations. This strategy will influence operational and financial aspects, in addition to energetic expenditures. Additional studies are required to determine the relevance of these aspects.

6. Outlook

Plant factories are just one example of trends in the development of novel (urban) functions that feature high internal heat loads. The presented study enabled us to quantify the role of façade construction in the total energy balance in plant factories and the potential for reduction of their energy use. The dissipation of heat across the façade proved to be the most efficient design strategy in terms of energy expenditure in the three locations. This passive approach limits the need for forced air extraction and cooling via climate systems and consequently reduces the electricity demand of such systems. In short, optimising the façade for the dissipation of the internal heat load results in the same total amount of heat being exhausted, but at a lower energy expenditure. The reuse of the excess energy for other (urban) functions is recommended as a topic for future study.

CRediT authorship contribution statement

Luuk Graamans: Conceptualization, Methodology, Software, Validation, Formal analysis, Investigation, Data curation, Writing - original draft, Writing - review & editing, Visualization. **Martin Tenpierik:** Conceptualization, Software, Formal analysis, Supervision, Writing - review & editing. **Andy den Dobbelsteen:** Supervision, Writing - review & editing. **Cecilia Stanghellini:** Supervision, Project administration, Writing - review & editing.

Declaration of Competing Interest

The authors declare that they have no known competing financial interests or personal relationships that could have appeared to influence the work reported in this paper.

Acknowledgements

This study was funded by the EU European Regional Development Fund "Kansen voor West" with the programme "Fieldlab FreshTeq". The authors wish to thank Staaij Food Group and Westland Infra for their support. Finally, the authors would like to express their gratitude to Mark Dornhelm for his advice on vapour compression cooling cycles and Dirk Hoogterp for his advice on heat exchangers.

Appendix A. – List of abbreviations and symbols

Nomenclature

Abbreviation	In model	Description	Unit
A	Albedo	Albedo: share diffuse reflection of total solar radiation	–
BWh	–	Köppen-Geiger: Hot desert climate	–
Cfb	–	Köppen-Geiger: Temperate oceanic climate	–
Dfc	–	Köppen-Geiger: Subarctic climate	–
HVAC	–	Heating, ventilation and air conditioning	–
NLD	NLD	the Netherlands	–
O	Opaque	Opaque	–
PPFD	PPFD	Photosynthetic photon flux density	μmol m^{-2} s^{-1}
SHGC	SHGC	Solar heat gain coefficient	–
SWE	SWE	Sweden	–
T	Transparent	Transparent	–
U-value	U	Heat transfer coefficient	W m^{-2} K^{-1}
UAE	UAE	the United Arab Emirates	–
W/F ratio	–	Wall-to-floor ratio	–

Symbols

Symbol	In model	Description	Unit
a	a	Thermal diffusivity of air	m^2 s^{-1}
A	A	Area of element a	m^2
COP	COP	Coefficient of performance	–
COP_{max}	COP_max	Coefficient of performance according to Carnot cycle	–
c_p	cp	Specific heat capacity	J kg^{-1} K^{-1}
E	E	Electricity use	kWhe
h	h	Enthalpy (of refrigerant unless specified otherwise)	kJ kg^{-1}
$\dot{m}$	m	Refrigerant mass flow rate	kg s^{-1}
n_{air}	n_air	Number of air exchanges	n h^{-1}
Nu	Nu	Nusselt number	–
p	p	Pressure	bar
Pr	Pr	Prandtl number	–
Q	Q	Energetic flux	kW
Re	Re	Reynolds number	–
RH_a	RH_a	Relative humidity at point a	%
s_a	s_a	Entropy of refrigerant at point a	kJ kg^{-1} K^{-1}
T	T	Temperature	°C
U	U	Heat transfer coefficient	W m^{-2} K^{-1}
u	u	Flow velocity	m^2 s^{-1}
V	V	Volumetric flow	m^3 s^{-1}
W_c	W_c	Compressor work input	kW
x	Ratio	Humidity ratio of moist air	kg kg^{-1}
α	alpha	Heat transfer coefficient	W m^{-2} K^{-1}
Δa	d_a	Difference in a	–
η_c	eta_c	Isentropic compressor efficiency	–
λ	lambda	Thermal conductivity	W m^{-1} K^{-1}
μ	mu	Dynamic viscosity	N s m^{-2}
ν	nu	Kinematic viscosity	m^2 s^{-1}
ρ_c,	rho	Density	kg m^{-3}
Φ'	phi_p	Heat transfer in tube	W m^{-1}
χ	x	Quality of fluid-vapour mixture	–

Subscripts

Subscript	In model	Description
$_0$	_0	of air entering the heat exchanger
$_1$	_1	of saturated vapour leaving the evaporator (including superheating)
$_{1s}$	_1s	of saturated vapour inside the evaporator
$_2$	_2	of superheated vapour leaving compressor (non-isentropic)
$_{2s}$	_2s	of superheated vapour leaving compressor (isentropic)
$_3$	_3	of saturated liquid leaving the condenser (including subcooling)
$_{3s}$	_3s	saturation at condenser
$_4$	_4	of liquid–vapour mixture exiting throttling process and entering evaporator
$_{air}$	_air	of air
$_{cool}$	_cool	cooling
$_{cond}$	_cond	at the condenser

evap	_evap	at the evaporator
ex	_ex	exterior
f4	_f4	of liquid refrigerant at T_4
fan	_fan	of a single fan
fans,a	_fans_a	of an array of fans for function a
fans,hex,a	_fans_hex_a	of an array of fans in the heat exchanger for function a
fl	_fl	due to friction loss
g4	_g4	of gas refrigerant at T_4
heat	_heat	heating
hex	_hex	of the heat exchanger
in	_in	interior
l	_L	at tube length l
lat	_lat	latent cooling
rc	_rc	refrigeration capacity
ref	_ref	reference
req	_req	required
sens	_sens	sensible cooling
set	_set	setpoint
sub	_sub	degree of subcooling
sup	_sup	degree of superheat
tot	_tot	total
w	_w	of water
we	_we	of the evaporation of water

Appendix B. – Resource use efficiency

Crop production should be calculated to ensure a clear comparison of resources expended for crop production, the resource use efficiency (Fig. B1). These values differ from the values in Fig. 6B due to the differences in plant production. The model described by Van Henten [34] was used to calculate plant production, following each interior climate. The implementation of this model was described by [8] and the presented calculations follow their assumptions on dry weight, root/shoot-ratio and dry matter content. The production cycle that yields the highest annual dry weight production per square metre was calculated for each interior climate dataset. A key boundary condition was a minimum fresh weight of 300 g per crop.

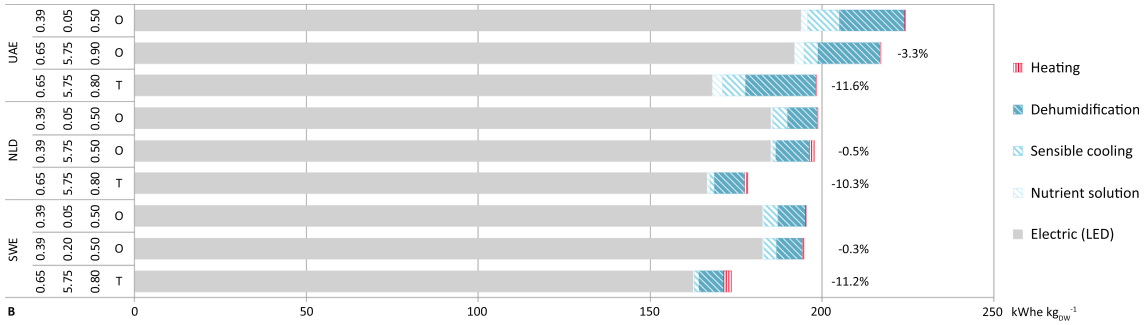

Fig. B1. Final electricity use for dry matter production (kWhe kg_{DW}^{-1}) for the most efficient opaque and transparent constructions in each location. The relative delta (%) illustrates the difference with the industry-standard plant factory in the specific location (opaque, U = 0.05 W m^{-2} K^{-1}, A = 0.55, W/F = 0.39). The y-axis lists location, W/F ratio (–), U-value (W m^{-2} K^{-1}), SGHC (–) or albedo (–) (dependent on transparency), and transparency (O for opaque and T for transparent) from left to right. The long façade faces north in presented simulations.

Appendix C. – Coefficients of performance

This section specifies the methodology applied to calculate the electricity requirement for cooling. The projected combination of active and 'free' cooling (Section 2.4) is explained and each individual technique is expanded upon. Active cooling was realised by a vapour compression refrigeration cycle and 'free' cooling was realised by an air-to-air heat exchanger. Other methods for 'free' cooling were considered unsuitable for this study, due to the direct disturbance to the indoor air quality (direct airside free cooling) or the need for elements closely tied to location, such as a large body of open water or a geothermal source (direct/indirect waterside free cooling).

The presented methodology is formulated as a general approach, limiting the need for technical details and system characteristics where possible. As input, the model uses the latent and sensible cooling load and the heating load from DesignBuilder. Additionally, the model requires the temperature and relative humidity of the supply air, the return air, and the exterior air. The calculations for the vapour compression cooling systems (C.1), the heat exchanger (C.2) and the forced air extraction (C.3) are detailed below.

C.1. – Active cooling: Vapour compression refrigeration cycle

In its most basic form, a vapour compression refrigeration system consists of an evaporator, a compressor, a condenser, a throttling device (which is usually an expansion valve or capillary tube) and the connecting tubing. The working fluid is the refrigerant, which goes through a thermodynamic cycle.

For each individual process type (and temperature range) there is a wide span of design parameters and configuration options, which should be evaluated in order to calculate the best available technology for the assignment in light of performance and investment [73]. As this level of detail

Table C1
Assumptions for vapour compression cycle.

Symbol	Value	Description	Source
T_{sup}	+5.0 K	Evaporator superheating	[73,78,79]
ΔT_{evap}	−8.0 K	Evaporator temperature off-set	[80]
T_{sub}	−9.0 K	Condenser subcooling	[81,82]
ΔT_{cond}	+15.0 K	Condenser temperature off-set	[74,82]
η_c	0.8	Compressor isentropic efficiency	[73,76]
R-	134A	Selected refrigerant	[76]

would go beyond the scope of this particular study, a model is constructed to calculate the performances under different operating conditions for the vapour compression model. This model is based on the fundamental principles of vapour compression cooling, as described by King [74], Zietlow [75] and Moran, Shapiro, Boettner & Bailey [76] and is explained in greater detail hereafter.

The calculation of the vapour compression cycle has four degrees of freedom: the superheat, subcooling, the condenser temperature and the evaporator temperature. The optimisation of the condenser and evaporator temperature offset does not entirely depend on the refrigeration cycle itself but depends on the ambient temperatures as well, due to the heat exchange [77].

Step 1: Fixing principal states

The heat transfers between the refrigerant and the warm and cold regions are not accomplished reversibly: the refrigerant temperature in the evaporator is lower than the cold region temperature ($T_{1s} < T_{evap,in}$) and the refrigerant temperature in the condenser is greater than the warm region temperature ($T_{3s} > T_{cond,in}$). An evaporator temperature difference (ΔT_{evap}) of 8 K with the interior air ($T_{evap,in}$) is assumed (see Table C1).

$$T_{1s} = T_{evap,in} + \Delta T_{evap} \tag{C.1}$$

The refrigerant is superheated (T_{sup}) beyond its boiling point to T_1 to ensure the quality of the vapour entering the compressor. T_{sup} is assumed to be 5 K.

$$T_1 = T_{1s} + T_{sup} \tag{C.2}$$

The enthalpy (h_1) and entropy (s_1) of the refrigerant entering the compressor can be determined following T_1 and the quality (x), which is a saturated vapour.

$$h_1 = h(T_1, x) \tag{C.3}$$

$$s_1 = s(T_1, x) \tag{C.4}$$

Step 2: Calculating the increase in entropy using compressor efficiency

A greater temperature difference between the condenser (T_{3s}) and the ambient air ($T_{cond,in}$) is required with an air-cooled condenser, to partially offset poor heat transfer through the air film. A temperature difference (ΔT_{cond}) of 15 K is assumed.

$$T_{3s} = T_{cond,in} + \Delta T_{cond} \tag{C.5}$$

The refrigerant is subcooled (T_{sub}) below its boiling point to T_3 to ensure the quality of the liquid refrigerant entering the expansion device. T_{sub} is assumed to be −9 K.

$$T_3 = T_{3s} + T_{sub} \tag{C.6}$$

The pressure at state-point 2 (p_2) is the same as the pressure at state-point 3 (p_3), which is the saturation pressure in the condenser, since constant pressure heat rejection in the condenser is assumed. The saturation pressure can be found using a property relationship as a function of the saturation temperature (T_{3s}).

$$p_2 = p_3 = p(T_{3s}) \tag{C.7}$$

In an isentropic process, which assumes an ideal compression, the entropy remains constant ($s_{2s} = s_1$). The enthalpy of the superheated vapour (h_{2s}) can then be determined using its entropy (s_1) and pressure (p_2) by:

$$h_{2s} = h(s_1, p_2) \tag{C.8}$$

In reality, the adiabatic compression process results in an increase in specific entropy from compressor inlet to exit due to irreversibilities. The isentropic compressor efficiency is given by:

$$\eta_c = \frac{h_{2s} - h_1}{h_2 - h_1} \quad \therefore \quad h_2 = \frac{h_{2s} - h_1}{\eta_c} + h_1 \tag{C.9}$$

The isentropic efficiency is one of the several parameters that typically has to be determined experimentally [83]. The presented model uses an efficiency of 0.8 (Table C1). State 2 is then fixed by the value of specific enthalpy h_2 and the pressure p_2, which makes it possible to determine the specific entropy (s_2):

$$s_2 = s(h_2, p_2) \tag{C.10}$$

Step 3: Determining condenser exit conditions, assuming a constant pressure

The quantity of refrigerant in the vapour compression cycle will determine the condition at the exit of the condenser. We assume that the amount of refrigerant provides a saturated liquid condition at the condenser exit and that pressure is kept constant. The specific enthalpy can then be approximated by the saturated liquid value. That is:

$$h(T, p) \approx h_f(T) \quad \therefore \quad h_3 \approx h_f(T_3) \tag{C.11}$$

The entropy of the saturated liquid exiting the condenser (h_3) can be approximated by the saturated liquid value at the given temperature.

$$s(T, p) \approx s_f(T) \quad \therefore \quad s_3 \approx s_f(T_3) \tag{C.12}$$

Step 4: Throttling process in expansion valve

The conservation of energy around the expansion device is used to find the specific enthalpy at state-point 4 (h_4) as a function of the specific enthalpy at state-point 3 (h_3). The expansion valve is considered adiabatic, so the throttling of the refrigerant at the expansion valve is considered to be isenthalpic [76].

$$h_4 = h_3 \tag{C.13}$$

The quality of the fluid-vapour mixture after the expansion valve can be calculated as follows:

$$\chi_4 = \frac{h_4 - h_{f4}}{h_{g4} - h_{f4}} \tag{C.14}$$

The enthalpy of saturated fluid is represented by h_f and h_g is the enthalpy of the saturated vapour. The specific entropy of the vapour-fluid mixture after the throttling valve (s_4) can then be calculated using the entropy of a saturated liquid (s_{f4}), a saturated gas (s_{g4}) and the quality of the vapour-fluid mixture (χ_4):

$$s_4 = s_{f4} + \chi_4 \cdot (s_{g4} - s_{f4}) \tag{C.15}$$

Step 5: Calculating cooling cycle characteristics

The required refrigerant mass flow rate ($\dot{m}$) is linked to the refrigeration capacity (Q_{rc}) required for the total cooling demand (Q_{tot}) and the change in enthalpy over the evaporator (h_1-h_4).

$$Q_{rc} = \dot{m}(h_1 - h_4) \quad \therefore \quad \dot{m} = \frac{Q_{rc}}{(h_1 - h_4)} \tag{C.16}$$

$$Q_{rc} = Q_{tot} \tag{C.17}$$

The mass flow rate and the heat of compression (h_2-h_1) can then be used to calculate the compressor power (W_c).

$$W_c = \dot{m}(h_2 - h_1) \tag{C.18}$$

The final coefficient of performance (COP) can be calculated using the refrigeration effect and the heat of compression.

$$COP = \frac{h_1 - h_4}{h_2 - h_1} \tag{C.19}$$

The total amount of heat rejected to the surrounding air is the heat lost in the condenser, Q_{cond} [82]. The amount of heat lost can be calculated using the refrigerant mass flow rate and the decrease in enthalpy (h_2-h_3).

$$Q_{cond} = \dot{m}(h_2 - h_3) \tag{C.20}$$

Step 6: Approximating physical system characteristics

From the conductance form of the equation it is possible to illustrate the relationship between the heat flux (Q_{cond} or Q_{evap}), the temperature difference (T_{3s}-$T_{cond,in}$ or T_{1s}-$T_{evap,in}$) and the design of the condenser or evaporator, as described in [75].

$$Q_{cond} = U_{cond} \cdot A_{cond} \cdot (T_{3s} - T_{cond,in}) \quad \therefore \quad U_{cond} \cdot A_{cond} = \frac{Q_{cond}}{(T_{3s} - T_{cond,in})} \tag{C.21}$$

$$Q_{evap} = U_{evap} \cdot A_{evap} \cdot (T_{1s} - T_{evap,in}) \quad \therefore \quad U_{evap} \cdot A_{evap} = \frac{Q_{evap}}{(T_{1s} - T_{evap,in})} \tag{C.22}$$

The overall conductance is the product of the overall heat transfer coefficient and the relevant heat transfer surface area (U·A), the latter comprising the exterior surface of the channels and fins. The overall heat transfer coefficient is fixed for a given cross-section of the channel, fin type, fin density and flow rates. An attempt to maximise the COP or minimize the irreversibilities results in the sizes of the heat exchangers approaching infinity [75]. These variables need to be determined by applying optimisation techniques which lie beyond the scope of this paper. The flow rates and expended energy for the forced ventilation are discussed in Section C.3.

C.2. – Free cooling: Air-to-air heat exchanger

An air-to-air heat exchanger is applied to make use of the exterior temperature as a cold source. For the vast majority of regions, the exterior temperature provides favourable conditions for free cooling for extended periods during the year [84]. Indirect air exchange takes advantage of favourable outdoor conditions without introducing outside air into the plant factory. The outside air which cools the extracted air is circulated through an independent loop, allowing for greater control of humidity and air quality [11].

Similar to the vapour compression cycle, there is a wide span of design parameters and configuration options. Providing this level of detail, however, would go beyond the scope of this study. A model is constructed to calculate the heat exchange under different operating conditions and is explained in greater detail hereafter.

Step 1: Determining ventilation requirement

The air volume flow extracted from the plant factory can be calculated using the total cooling demand (Q_{tot}), the density ($\rho_{c,in}$) and specific heat capacity ($c_{p,in}$) of the interior air, as well as the difference in enthalpy with the exterior air (Δh_{air}). The flow velocity ($u_{air,in}$) is determined by the hydraulic inner radius of the cylindrical tube (r_{in}) and the volume air flow (V_{air}).

$$V_{air} = \frac{Q_{tot}}{\rho_{c,in} \cdot \Delta h_{air}} \tag{C.23}$$

$$u_{air,in} = \frac{V_{air}}{\pi \cdot (r_{in})^2} \quad \therefore \quad r_{in} = \sqrt{\frac{V_{air}}{u_{air,in} \cdot \pi}} \tag{C.24}$$

$$V_{air,hex,ref} = \frac{Q_{cool,ref}}{\Delta h_{evap,ref} \cdot \rho_{c,air,ref} \cdot n_{hex}} \tag{C.25}$$

The required r_{in} can be estimated taking a reference volume air flow ($V_{air,hex,ref}$), a maximum $u_{air,in}$, the difference in enthalpy between supply air and return air ($\Delta h_{evap,ref}$) and the number of parallel heat exchanger arrays (n_{hex}) (see also Table C2). The enthalpy of moist air (h_{air}) is determined using air temperature (T_{air}), the specific heat of air and water ($c_{p,air}$ and $c_{p,w}$, respectively) and the evaporation heat of water (h_{we}), as described in [86].

$$h_{air} = c_{p,air} \cdot T_{air} + x_{air} \cdot (h_{we} + c_{p,w} \cdot T_{air}) \tag{C.26}$$

In order to prevent excessive u_{air} it is recommended to split the extracted V_{air} over multiple vents. This also minimises vent diameters.

Step 2: Calculating heat transfer inside the tube

In order to calculate the total heat transfer it is necessary to determine the transfer from the air inside the tube to the tube itself, as well as the transfer from the tube surface to the surrounding air. Firstly, the exchange between the interior medium and the tube is calculated. The turbulence of the flow is dependent on the Reynolds number (Re_{in}), which is comprised of $\rho_{c,in}$, $u_{air,in}$, and the dynamic viscosity of the air in the tube (μ_{in}), after [87].

$$Re_{in} = \frac{\rho_{c,air,in} \cdot u_{air,in} \cdot 2 \cdot r_{in}}{\mu_{air,in}} \tag{C.27}$$

The heat transfer between the medium inside the tube and the tube surface under turbulent flow regime is governed by the Nusselt number (Nu_{in}), which is a function of the Prandtl (Pr) and Reynolds (Re) numbers. Pr is the product of the kinematic viscosity (ν) and the thermal diffusivity (a) of air [88]. The function for turbulent flow in a smooth tube is given by [89].

$$Pr = \frac{\nu}{a} \tag{C.28}$$

$$Nu_{in} = 0.023 \cdot Re_{in}^{0.8} \cdot Pr^{0.4} \tag{C.29}$$

The heat transfer coefficient between the air inside the tube and the tube surface (α_{in}) is determined using Nu_{in}, r_{in} and the thermal conductivity of the interior air ($\lambda_{air,in}$).

$$\alpha_{in} = \frac{Nu_{in} \cdot \lambda_{air,in}}{2 \cdot r_{in}} \tag{C.30}$$

Table C2
Assumptions for heat exchanger and ventilation.

Symbol	Value	Description	Source
n_{hex}	20	Number of parallel heat exchanger arrays	–
λ_{tube}	380 W m^{-1} K^{-1}	Thermal conductivity of copper tube	[51]
d_{tube}	0.0015 m	Tube wall thickness	–
$Q_{cool,ref}$	750 kW	Reference volume air flow	Output: maximum cooling demand
$u_{air,max}$	15 m s^{-1}	Maximum air speed in vents	[85]

Step 3: Calculating heat transfer from the tube

Secondly, the heat transfer between the tube surface and the surrounding air is calculated. The heat transfer coefficient is determined by Nu, as in Eq. (C.30), which depends on the Reynolds (Re_{ex}) and Prandtl (Pr_{ex}) numbers, accounting for the exterior air characteristics $\rho_{c,ex}$, $u_{air.ex}$, and μ_{ex}, and the exterior tube radius (r_{ex}).

$$Re_{ex} = \frac{\rho_{c,ex} \cdot u_{air,ex} \cdot 2r_{ex}}{\mu_{air,ex}} \tag{C.31}$$

Assuming that external air is not under pressure, Pr_{ex} can be regarded as constant, and is incorporated into the coefficient of the corresponding formula in Eq. (C.29) [90].

$$Nu_{ex} = 0.023 \cdot Re_{ex}^{0.8} \tag{C.32}$$

The heat transfer coefficient between the tube surface and the surrounding air (α_{ex}) is determined as in Eq. (C.30), using Nu_{ex}, r_{ex} and the thermal conductivity of the exterior air ($\lambda_{air,ex}$).

$$\alpha_{ex} = \frac{Nu_{ex} \cdot \lambda_{air,ex}}{2 \cdot r_{ex}} \tag{C.33}$$

Step 4: Calculating total heat transfer

The heat transfer (Φ') in W m^{-1} can be calculated following the temperature difference between the air temperature at position l in the tube (T_l) and the exterior air ($T_{air,ex}$), the various thermal conductivities and the tube dimensions.

$$\Phi' = \frac{(T_l - T_{air,ex})}{\left(\frac{1}{\alpha_{in} \cdot 2 \cdot \pi \cdot r_{in}} + \frac{1}{\alpha_{ex} \cdot 2 \cdot \pi \cdot r_{ex}} + \frac{\ln(r_{ex} / r_{in})}{2 \cdot \pi \cdot \lambda}\right)} \tag{C.34}$$

The temperature of the air after tube length l (T_l) can be calculated using the various resistances, the air temperature at the start of the tube (T_0), the tube length l, the surface area of the cross-section, as well as the air characteristics.

$$T_l = T_{air,ex} + (T_0 - T_{air,ex}) \cdot e^{-\frac{l}{R' \cdot \rho_{c,air,in} \cdot c_{p,air,in} \cdot u_{air,in} \cdot \pi \cdot (r_{in})^2}} \tag{C.35}$$

where:

$$R' = \frac{1}{\alpha_{in} \cdot 2 \cdot \pi \cdot r_{in}} + \frac{1}{\alpha_{ex} \cdot 2 \cdot \pi \cdot r_{ex}} + \frac{\ln(r_{ex}/r_{in})}{2 \cdot \pi \cdot \lambda} \tag{C.36}$$

where l is either the maximum tube length (l_{max} = 40 m, see Table C2) or the required tube length (l_{req}) to reach the temperature setpoint for the supply air (18 °C). Variable l_{req} is determined by:

$$l_{req} = -\ln\left(\frac{T_{l,set} - T_{air}}{T_0 - T_{air}}\right) \cdot (R' \cdot \rho_{c,in} \cdot c_p \cdot u_{air} \cdot \pi \cdot (r_{in})^2) \tag{C.37}$$

The latent and sensible component ($Q_{hex,lat}$ and $Q_{hex,sens}$, respectively) of the energy exchanged are determined as follows:

$$Q_{hex,lat} = \Delta x_{air,hex} \cdot h_{we} \cdot \rho_{c,air} \cdot V_{air} \tag{C.38}$$

$$Q_{hex,sens} = \Delta h_{air,hex} \cdot \rho_{c,air} \cdot V_{air} - Q_{hex,lat} \tag{C.39}$$

The presented model can be used to calculate the potential heat transfer to the surrounding environment, without requiring active cooling. The total heat transfer is dominated by the exchange with the surrounding air, which is facilitated by forced ventilation (see Section C.3). The emissivity to the night's sky is not considered as heat exchangers are typically built to be compact, decreasing the relative importance of radiation in the cooling process.

C.3. – Active and free cooling: Forced ventilation

Air circulation fans are required for an adequate exchange between the evaporator, the condenser, the heat exchanger and the surrounding air. These fans represent a notable share in the total electricity requirement for cooling [59]. The required electricity for forced ventilation (fan power) was determined based on [82]. The methodology is specified hereafter.

The power input of (condenser) fans ($P_{fan,elec}$) means the total power of the fan(s) staged at a given operating condition. The necessary mechanical fan power ($P_{fan,mech}$) can be determined from the volume flow of air (V_{air}) and the pressure difference (Δp), assuming an incompressible flow [78].

$$P_{fan,mech} = V_{air} \cdot \Delta p \tag{C.40}$$

In order to include both the sensible and the latent component, we use the difference in enthalpy to determine V_{air}, as is shown in Eq. (C.23). To prevent excessive fan dimensions, it is recommended to split the extracted V_{air} over multiple fans. The Δp can be found using the Bernoulli equation, air characteristics and the friction loss (Δp_{fl}).

$$\Delta p = \frac{u_{air}^2 \cdot \rho_{c,air}}{2} + \Delta p_{fl} \tag{C.41}$$

The Δp_{fl} can be defined as a function of u_{air} [78]:

$$\Delta p_{fl} = 3.4 \cdot u_{air}^2 + 4.9 \cdot u_{air} \quad \text{(C.42)}$$

The expended electrical power (E_{fans}) can then be calculated when introducing a fan efficiency (η_{fan}).

$$E_{fans} = \frac{V_{air}}{\eta_{fan}} \cdot \left(\frac{\rho_{c,air} \cdot u_{air}^2}{2} + \Delta p_{fl}\right) \quad \text{(C.43)}$$

In the presented calculations η_{fan} was assumed to be 65%, in line with [78]. The electricity expenditure of the fans ($E_{fans,a}$) is specified for heating and sensible and latent cooling by its relative share (Q_a) in the total energy demand.

$$E_{fans,a} = \frac{Q_a}{Q_{lat} + Q_{sens} + Q_{heat}} \cdot E_{fans} \quad \text{(C.44)}$$

A similar method is applied to specify the electricity expenditure of the heat exchanger fans ($E_{fans,hex,a}$) for sensible and latent cooling ($Q_{hex,sens}$ and $Q_{hex,lat}$, respectively).

$$E_{fans,hex,a} = \frac{Q_a}{Q_{lat} + Q_{sens}} \cdot E_{fans,hex} \quad \text{(C.45)}$$

Appendix D. Supplementary material

Supplementary data to this article can be found online at https://doi.org/10.1016/j.apenergy.2020.114544.

References

[1] Benis K, Ferrão P. Commercial farming within the urban built environment – taking stock of an evolving field in northern countries. Global Food Secur 2018;17:30–7. https://doi.org/10.1016/j.gfs.2018.03.005.

[2] Kennedy C, Cuddihy J, Engel-Yan J. The changing metabolism of cities. J Ind Ecol 2007;11(2):43–59. https://doi.org/10.1162/jiec.0.1107.

[3] Newcombe K, Nichols EH. An integrated ecological approach to agricultural policy-making with reference to the urban fringe: the case of Hong Kong. Agric Syst 1979;4(1):1–27. https://doi.org/10.1016/0308-521x(79)90011-8.

[4] United Nations. World urbanization prospects: The 2014 revision, highlights. New York: United Nations – Department of Economic and Social Affairs – Population division; 2014. doi: 10.18356/527e5125-en.

[5] Seginer I, Ioslovich I. Optimal spacing and cultivation intensity for an industrialized crop production system. Agric Syst 1999;62(3):143–57. https://doi.org/10.1016/s0308-521x(99)00057-8.

[6] Kozai T, Ohyama K, Chun C. Commercialized closed systems with artificial lighting for plant production. Acta Hortic 2006;711:61–70. https://doi.org/10.17660/actahortic.2006.711.5.

[7] Kozai T. Resource use efficiency of closed plant production system with artificial light: concept, estimation and application to plant factory. Proc Jpn Acad B Phys Biol Sci 89(10), 447-461. doi: 10.2183/pjab.89.447.

[8] Graamans L, Baeza E, van den Dobbelsteen AAJF, Tsafaras I, Stanghellini C. Plant factories versus greenhouses: comparison of resource use efficiency. Agric Syst 2018;160:31–43. https://doi.org/10.1016/j.agsy.2017.11.003.

[9] Kozai T. Sustainable plant factory: closed plant production systems with artificial light for high resource use efficiencies and quality produce. Acta Hortic 2013;1004:27–40. https://doi.org/10.17660/actahortic.2013.1004.2.

[10] Graamans L, van den Dobbelsteen AAJF, Meinen E, Stanghellini C. Plant factories; crop transpiration and energy balance. Agric Syst 2017;153:138–47. https://doi.org/10.1016/j.agsy.2017.01.003.

[11] Daraghmeh HM, Wang CC. A review of current status of free cooling in datacenters. Appl Therm Eng 2017;114:1224–39. https://doi.org/10.1016/j.applthermaleng.2016.10.093.

[12] Boyano A, Hernandez P, Wolf O. Energy demands and potential savings in European office buildings: case studies based on EnergyPlus simulations. Energy Build 2013;65:19–28. https://doi.org/10.1016/j.enbuild.2013.05.039.

[13] Ihara T, Gustavsen A, Jelle BP. Effect of facade components on energy efficiency in office buildings. Appl Energy 2015;158:422–32. https://doi.org/10.1016/j.apenergy.2015.08.074.

[14] Hien WN, Liping W, Chandra AN, Pandey AR, Xiaolin W. Effects of double glazed facade on energy consumption, thermal comfort and condensation for a typical office building in Singapore. Energy Build 2005;37(6):563–72. https://doi.org/10.1016/j.enbuild.2004.08.004.

[15] Thalfeldt M, Pikas E, Kurnitski J, Voll H. Facade design principles for nearly zero energy buildings in a cold climate. Energy Build 2013;67:309–21. https://doi.org/10.1016/j.enbuild.2013.08.027.

[16] Khalaj AH, Halgamuge SK. A review on efficient thermal management of air-and liquid-cooled data centers: from chip to the cooling system. Appl Energy 2017;205:1165–88. https://doi.org/10.1016/j.apenergy.2017.08.037.

[17] Cho J, Kim Y. Improving energy efficiency of dedicated cooling system and its contribution towards meeting an energy-optimized data center. Appl Energy 2016;165:967–82. https://doi.org/10.1016/j.apenergy.2015.12.099.

[18] Oró E, Depoorter V, Pflugradt N, Salom J. Overview of direct air free cooling and thermal energy storage potential energy savings in data centres. Appl Therm Eng 2015;85:100–10. https://doi.org/10.1016/j.applthermaleng.2015.03.001.

[19] Crawley DB, Lawrie LK, Winkelmann FC, Buhl WF, Huang YJ, Pedersen CO, et al. EnergyPlus: creating a new-generation building energy simulation program. Energy Build 2001;33(4):319–31. https://doi.org/10.1016/s0378-7788(00)00114-6.

[20] Witte MJ, Henninger RH, Glazer J, Crawley DB. Testing and validation of a new building energy simulation program. Paper presented at the 7th International Building Performance Simulation Association Conference, Rio de Janeiro, Brazil. 2001.

[21] Raji B, Tenpierik MJ, van den Dobbelsteen AAJF. An assessment of energy-saving solutions for the envelope design of high-rise buildings in temperate climates: a case study in the Netherlands. Energy Build 2016;124:210–21. https://doi.org/10.1016/j.enbuild.2015.10.049.

[22] Shrestha SS, Maxwell G. Empirical validation of building energy simulation software: EnergyPlus. Paper presented at the 12th Conference of International Building Performance Simulation Association, Sydney, Australia; 2011.

[23] Loutzenhiser PG, Manz H, Moosberger S, Maxwell GM. An empirical validation of window solar gain models and the associated interactions. Int J Therm Sci 2009;48(1):85–95. https://doi.org/10.1016/j.ijthermalsci.2008.01.011.

[24] Arasteh D, Kohler C, Griffith B. Modeling windows in energy plus with simple performance indices; 2009. doi:10.2172/975375.

[25] Fumo N, Mago P, Luck R. Methodology to estimate building energy consumption using EnergyPlus Benchmark Models. Energy Build 2010;42(12):2331–7. https://doi.org/10.1016/j.enbuild.2010.07.027.

[26] Anđelković AS, Mujan I, Dakić S. Experimental validation of a EnergyPlus model: application of a multi-storey naturally ventilated double skin façade. Energy Build 2016;118:27–36. https://doi.org/10.1016/j.enbuild.2016.02.045.

[27] Crawley DB. Which weather data should you use for energy simulations of commercial buildings? ASHRAE Trans 1998;104:498–515.

[28] ASHRAE. ASHRAE Standard 140-2011. Standard method of test for the evaluation of building energy analysis computer programs. Atlanta, USA: ASHRAE – American Society of Heating, Refrigerating and Air-Conditioning Engineers; 2011.

[29] DesignBuilder. DesignBuilder version 5.3.0.014. Glouchestershire, UK: DesignBuilder Software Ltd.; 2018 Retrieved from www.designbuilder.co.uk/index.php.

[30] De Zwart HF. Analyzing energy-saving options in greenhouse cultivation using a simulation model. (PhD), Wageningen University & Research, Wageningen, the Netherlands; 1996.

[31] Tei F, Scaife A, Aikman DP. Growth of lettuce, onion, and red beet. 1. Growth analysis, light interception, and radiation use efficiency. Ann Bot 1996;78(5):633–43. https://doi.org/10.1006/anbo.1996.0171.

[32] De Visser PHB, van der Heijden G, Buck-Sorlin G. Optimizing illumination in the greenhouse using a 3D model of tomato and a ray tracer. Front Plant Sci 2014;5:48. https://doi.org/10.3389/fpls.2014.00048.

[33] Farquhar GD, von Caemmerer S, Berry JA. A biochemical model of photosynthetic CO_2 assimilation in leaves of C_3 species. Planta 1980;149(1):78–90. https://doi.org/10.1007/bf00386231.

[34] Van Henten EJ. Validation of a dynamic lettuce growth model for greenhouse climate control. Agric Syst 1994;45(1):55–72. https://doi.org/10.1016/S0308-521X(94)90280-1.

[35] MATLAB. MATLAB version R2018a (9.4.0.813654). Natick, Massachusetts, USA: The MathWorks, Inc; 2018. Retrieved from www.mathworks.com/products/matlab.html.

[36] Van Henten EJ, Van Straten G. Sensitivity analysis of a dynamic growth model of lettuce. J Agric Eng Res 1994;59(1):19–31. https://doi.org/10.1006/jaer.1994.

1061.
[37] EnergyPlus. EnergyPlus weather data by location - Abu Dhabi 412170 (IWEC); 2018. Retrieved 30 April 2018 https://energyplus.net/weather-download/asia_wmo_region_2/ARE//ARE_Abu.Dhabi.412170_IWEC/ARE_Abu.Dhabi.412170_IWEC.
[38] EnergyPlus. EnergyPlus weather data by location – Amsterdam 062400 (IWEC); 2018. Retrieved 26 April 2018 https://energyplus.net/weather-location/europe_wmo_region_6/NLD//NLD_Amsterdam.062400_IWEC.
[39] EnergyPlus. EnergyPlus weather data by location - Kiruna 020440 (IWEC); 2018. Retrieved 30 April 2018 https://energyplus.net/weather-location/europe_wmo_region_6/SWE//SWE_Kiruna.020440_IWEC.
[40] Zhang X, He DX, Niu GH, Yan ZN, Song JX. Effects of environment lighting on the growth, photosynthesis, and quality of hydroponic lettuce in a plant factory. Int J Agric Biol Eng 2018;11(2):33–40. https://doi.org/10.25165/j.ijabe.20181102.3240.
[41] Fu WG, Li PP, Wu YY. Effects of different light intensities on chlorophyll fluorescence characteristics and yield in lettuce. Sci Hortic 2012;135:45–51. https://doi.org/10.1016/j.scienta.2011.12.004.
[42] Hiroki R, Shimizu H, Ito A, Nakashima H, Miyasaka J, Ohdoi K. Identifying the optimum light cycle for lettuce growth in a plant factory. Paper presented at the International Symposium on New Technologies for Environment Control, Energy-Saving and Crop Production in Greenhouse and Plant Factory - Greensys 2013; 2013.
[43] Lee HI, Kim YH. Utilization efficiencies of electric energy and photosynthetically active radiation of lettuce grown under red LED, blue LED and fluorescent lamps with different photoperiods. J Biosyst Eng 2013;38(4):279–86. https://doi.org/10.5307/jbe.2013.38.4.279.
[44] Waycott W. Photoperiodic response of genetically diverse lettuce accessions. J Am Soc Hortic Sci 1995;120(3):460–7.
[45] Hall AE. A model of leaf photosynthesis and respiration for predicting carbon dioxide assimilation in different environments. Oecologia 1979;43(3):299–316. https://doi.org/10.1007/bf00344957.
[46] He J, Lee SK. Growth and photosynthetic responses of three aeroponically grown lettuce cultivars (*Lactuca sativa* L.) to different rootzone temperatures and growth irradiances under tropical aerial conditions. J Hortic Sci Biotechnol 1998;73(2):173–80. https://doi.org/10.1080/14620316.1998.11510961.
[47] Thompson HC, Langhans RW, Both AJ, Albright LD. Shoot and root temperature effects on lettuce growth in a floating hydroponic system. J Am Soc Hortic Sci 1998;123(3):361–4.
[48] Frantz JM, Ritchie G, Cometti NN, Robinson J, Bugbee B. Exploring the limits of crop productivity: beyond the limits of tipburn in lettuce. J Am Soc Hortic Sci 2004;129(3):331–8.
[49] Tenpierik MJ, Cauberg JJM, Thorsell TI. Integrating vacuum insulation panels in building constructions: an integral perspective. Construction Innovation 2007;7(1):38–53. https://doi.org/10.1108/14714170710721287.
[50] Engineering ToolBox. (2004). Transmission heat loss through building elements. Retrieved 21 May 2019 https://www.engineeringtoolbox.com/heat-loss-transmission-d_748.html.
[51] Engineering ToolBox. (2005). Thermal conductivity of metals, metallic elements and alloys. Retrieved 19 August 2019 https://www.engineeringtoolbox.com/thermal-conductivity-metals-d_858.html.
[52] Jelle BP, Gustavsen A, Baetens R. The path to the high performance thermal building insulation materials and solutions of tomorrow. J Build Phys 2010;34(2):99–123. https://doi.org/10.1177/1744259110372782.
[53] Ihara T, Gao T, Grynning S, Jelle BP, Gustavsen A. Aerogel granulate glazing facades and their application potential from an energy saving perspective. Appl Energy 2015;142:179–91. https://doi.org/10.1016/j.apenergy.2014.12.053.
[54] Gao T, Jelle BP, Sandberg LIC, Gustavsen A. Monodisperse hollow silica nanospheres for nano insulation materials: synthesis, characterization, and life cycle assessment. ACS Appl Mater Interfaces 2013;5(3):761–7. https://doi.org/10.1021/am302303b.
[55] Engineering ToolBox. (2012). Materials - Light reflecting factors. Retrieved 22 December 2019 https://www.engineeringtoolbox.com/light-material-reflecting-factor-d_1842.html.
[56] United States – Department of Energy. EnergyPlus documentation – Input output reference. Berkeley, CA (USA); 2018.
[57] United States – Department of Energy. EnergyPlus documentation – Engineering reference. Berkeley, CA (USA); 2015.
[58] Meggers F, Ritter V, Goffin P, Baetschmann M, Leibundgut H. Low exergy building systems implementation. Energy 2012;41(1):48–55. https://doi.org/10.1016/j.energy.2011.07.031.
[59] Bieliński H, Mikielewicz J. Natural circulation in single and two phase thermosyphon loop with conventional tubes and minichannels. In: Belmiloudi, A. (Ed.), Heat transfer - Mathematical modelling, numerical methods and information technology: Intech; 2011. doi:10.5772/569.
[60] Sabharwall P, Patterson M, Gunnerson F. Theoretical design of thermosyphon for process heat transfer from NGNP to hydrogen plant. Paper presented at the ASME 4th International Topical Meeting on High Temperature Reactor Technology, Washington, D.C., USA; 2008.
[61] Haider SI, Joshi YK, Nakayama W. A natural circulation model of the closed loop, two-phase thermosyphon for electronics cooling. J Heat Transfer 2002;124(5):881–90. https://doi.org/10.1115/1.1482404.
[62] Milanez F, Mantelli MBH. Heat transfer limit due to pressure drop of a two-phase loop thermosyphon. Heat Pipe Sci Technol An Int J 2010;1(3). https://doi.org/10.1615/heatpipescietech.2011003082.
[63] Zhang H, Shao S, Xu H, Zou H, Tang M, Tian C. Simulation on the performance and free cooling potential of the thermosyphon mode in an integrated system of mechanical refrigeration and thermosyphon. Appl Energy 2017;185:1604–12. https://doi.org/10.1016/j.apenergy.2016.01.053.
[64] Lee S, Kang H, Kim Y. Performance optimization of a hybrid cooler combining vapor compression and natural circulation cycles. Int J Refrig 2009;32(5):800–8. https://doi.org/10.1016/j.ijrefrig.2008.12.008.
[65] Gartia MR, Vijayan PK, Pilkhwal DS. A generalized flow correlation for two-phase natural circulation loops. Nucl Eng Des 2006;236(17):1800–9. https://doi.org/10.1016/j.nucengdes.2006.02.004.
[66] Nishimura M, Kozai T, Kubota C, Chun C. Analysis of electric energy consumption and its cost for a closed-type transplant production system. J Soc High Technol Agric 2001;14(3):204–9.
[67] Ohyama K, Kozai T, Kubota C, Chun C, Hasegawa T, Yokoi S, et al. Coefficient of performance for cooling of a home-use air conditioner installed in a closed-type transplant production system. Shokubutsu Kojo Gakkaishi 2002;14(3):141–6. https://doi.org/10.2525/jshita.14.141.
[68] Tong Y, Yang Q, Shimamura S. Analysis of electric-energy utilization efficiency in a plant factory with artificial light for lettuce production. Paper presented at the International Symposium on New Technologies for Environment Control, Energy-Saving and Crop Production in Greenhouse and Plant Factory – Greensys; 2013.
[69] Harbick K, Albright LD. Comparison of energy consumption: greenhouses and plant factories. Acta Hortic 2016;1134:285–92. https://doi.org/10.17660/actahortic.2016.1134.38.
[70] Pattison PM, Hansen M, Tsao JY. LED lighting efficacy: status and directions. CR Phys 2018;19(3):134–45. https://doi.org/10.1016/j.crhy.2017.10.013.
[71] Tyagi VV, Rahim NAA, Rahim NA, Selvaraj JAL. Progress in solar PV technology: research and achievement. Renew Sustain Energy Rev 2013;20(C):443–61. https://doi.org/10.1016/j.rser.2012.09.028.
[72] Royal Philips NV. Philips GreenPower LED production module.; 2018 Retrieved 15 October 2018 http://www.lighting.philips.com/main/products/horticulture/products/greenpower-led-production-module.
[73] Ommen T, Jensen JK, Markussen WB, Reinholdt L, Elmegaard B. Technical and economic working domains of industrial heat pumps: Part 1–Single stage vapour compression heat pumps. Int J Refrig 2015;55:168–82. https://doi.org/10.1016/j.ijrefrig.2015.02.012.
[74] King GR. Modern refrigeration practice. McGraw-Hill Companies; 1971.
[75] Zietlow DC Optimization of vapor compression cycles. Paper presented at the American Society for Engineering Education, Indianapolis, IN, USA; 2014.
[76] Moran MJ, Shapiro HN, Boettner DD, Bailey MB. Principles of Engineering Thermodynamics, 8th Edition - SI Version. John Wiley & Sons; 2015.
[77] Larsen LS, Thybo C. Potential energy savings in refrigeration systems using optimal set-points. Paper presented at the IEEE International Conference on Control Applications; 2004.
[78] Sahlsten A, Heinerud V. Natural refigerants in data center cooling with thermosiphon application. (MSc), KTH, Stockholm, Sweden; 2016.
[79] Kim DH, Park HS, Kim MS. Optimal temperature between high and low stage cycles for R134a/R410A cascade heat pump based water heater system. Exp Therm Fluid Sci 2013;47:172–9. https://doi.org/10.1016/j.expthermflusci.2013.01.013.
[80] Maivel M, Kurnitski J. Heating system return temperature effect on heat pump performance. Energy Build 2015;94:71–9. https://doi.org/10.1016/j.enbuild.2015.02.048.
[81] Pottker G, Hrnjak P. Effect of the condenser subcooling on the performance of vapor compression systems. Int J Refrig 2015;50:156–64. https://doi.org/10.1016/j.ijrefrig.2014.11.003.
[82] Chan KT, Yu FW. Optimum setpoint of condensing temperature for air-cooled chillers. HVAC&R Res 2004;10(2):113–27. https://doi.org/10.1080/10789669.2004.10391095.
[83] Zsembinszki G, de Gracia A, Moreno P, Rovira R, González MA, Cabeza LF. A novel numerical methodology for modelling simple vapour compression refrigeration system. Appl Therm Eng 2017;115:188–200. https://doi.org/10.1016/j.applthermaleng.2016.12.059.
[84] Zhang H, Shao S, Xu H, Zou H, Tian C. Free cooling of data centers: a review. Renew Sustain Energy Rev 2014;35:171–82. https://doi.org/10.1016/j.rser.2014.04.017.
[85] Engineering ToolBox. (2005). Air duct velocities. Retrieved 21 August 2019 https://www.engineeringtoolbox.com/duct-velocity-d_928.html.
[86] Engineering ToolBox. Enthalpy of moist air. Retrieved 21 August 2019; 2004 https://www.engineeringtoolbox.com/enthalpy-moist-air-d_683.html.
[87] Rattner A, Bohren J. Heat and mass correlations. from University of Pennsylvania; 2008.
[88] Van Wijngaarden L. Warmte- en stromingsleer - deel 1b. from Universiteit Twente; 1971.
[89] Holman JP. Heat transfer. 8th ed. New York, NY, USA: McGraw-Hill; 1997.
[90] Kutateladze SS. Fundamentals of Heat Transfer. London, UK: Edward Arnold; 1963.